lubricants

MDPI

Review

Toward Reliable Triboelectric Nanogenerators: Roles of Lubricants

P. R. Deshmukh [1] and Dae-Hyun Cho [2,3,*]

[1] Future Convergence Technology Research Institute, Gyeongsang National University, Jinju 52725, Gyeongnam, Republic of Korea; dprashant@gnu.ac.kr
[2] Department of Mechatronics Engineering, Gyeongsang National University, Jinju 52725, Gyeongnam, Republic of Korea
[3] Department of Energy System Engineering, Gyeongsang National University, Jinju 52828, Gyeongnam, Republic of Korea
* Correspondence: cho@gnu.ac.kr; Tel.: +82-55-772-3387; Fax: +82-55-751-3389

Abstract

Triboelectric nanogenerators (TENGs) are a newly adopted technology designed to harvest freely available mechanical energy from the environment and convert it into electricity that can help to meet future demands for clean and sustainable energy. TENGs represent a promising next-generation renewable energy technology, an alternative to traditional non-renewable fossil fuel sources, with a wide range of applications, including smart sensors, wearable devices, internet of things (IoT), and portable electronics. Through contact/triboelectrification and electrostatic induction, TENGs convert mechanical energy into electrical energy. Broadly, TENGs are classified into contact–separation mode and sliding mode. In contact–separation mode, the electric output is achieved through the contact and separation of triboelectric layers, while in the sliding mode, it is generated by the sliding of one triboelectric layer over another. Sliding-mode TENGs have demonstrated better electrical output compared to the contact–separation mode; however, they suffer low durability and cannot operate for long periods due to severe wear. In addition, their electrical output performance is reduced owing to air breakdown. Lubricants have demonstrated their potential in TENGs by overcoming these limitations and improving both tribological and triboelectric performance. This review provides a discussion on the fundamental modes of TENGs, followed by a comprehensive summary of the tribological and triboelectrical performance of existing TENGs under liquid lubrication, along with a comparison of their performance under dry conditions. The effects of load, frequency, mass fraction, and volume of the liquid lubricant on both tribology and electrical output are examined. Durability is identified as a key factor for the long-term practical application of TENGs; hence, this paper also focuses on it. Furthermore, strategies for improving TENG performance and the working mechanisms under liquid lubrication are discussed. Finally, the paper summarizes demonstrations of TENG applications based on various TENG designs.

Keywords: triboelectric nanogenerators; mechanical energy; electrical energy; power; liquid lubricant; durability; application demonstration

Check for updates

Received: 18 December 2025
Revised: 28 January 2026
Accepted: 3 February 2026
Published: 10 February 2026

Copyright: © 2026 by the authors. Licensee MDPI, Basel, Switzerland. This article is an open access article distributed under the terms and conditions of the Creative Commons Attribution (CC BY) license.

1. Introduction

The escalating global energy crisis and environmental degradation, driven by rising energy demands and the excessive reliance on non-renewable fossil fuels, such as natural

gas, coal, and oil, have intensified the search for sustainable alternatives [1–4]. Renewable sources, such as wind, solar, ocean, and mechanical energy, are abundant, clean, and environmentally safe, making them attractive candidates for long-term energy solutions [4–8]. Among these, mechanical energy harvested from ambient environments has emerged as particularly promising due to its ubiquity and independence from external conditions such as weather and temperature [1–8]. In recent years, triboelectric nanogenerators (TENGs), first introduced by Fan et al. in 2012 [9], have gained significant attention as an innovative technology for converting mechanical energy into electrical energy through triboelectrification and electrostatic induction mechanisms. It is a prevailing technology that converts irregular, low-frequency, and randomly distributed waste energy from the environment into useful electric energy [10–13]. TENGs can efficiently capture wasted mechanical energy from human motion, frictional processes, rotations, and even large-scale sources, such as ocean waves, rain, and wind, offering broad applications in stable energy supply, sensors, robotics, artificial intelligence, and self-powered microelectronic devices [14–17]. For example, TENG applications in self-powered electronic devices include microreactor and microfluidic transport systems. TENGs generate a very high open-circuit voltage (~kV), while producing a very low short-circuit current (~microampere or milliampere). Taking advantage of this high-voltage source, TENGs have integrated with microreactor and microfluidic systems for droplet manipulation in non-air environments, driving micro reactions in oil media and transporting tiny droplets across both horizontal and vertical planes [18,19]. TENGs' simple fabrication, low cost, lightweight, flexible structural design, eco-friendliness, wide range of material options, and compatibility with diverse materials have enabled TENGs to represent a reliable and cost-effective pathway toward sustainable energy harvesting [20–22]. Figure 1a displays an overview of TENG applications and advantages.

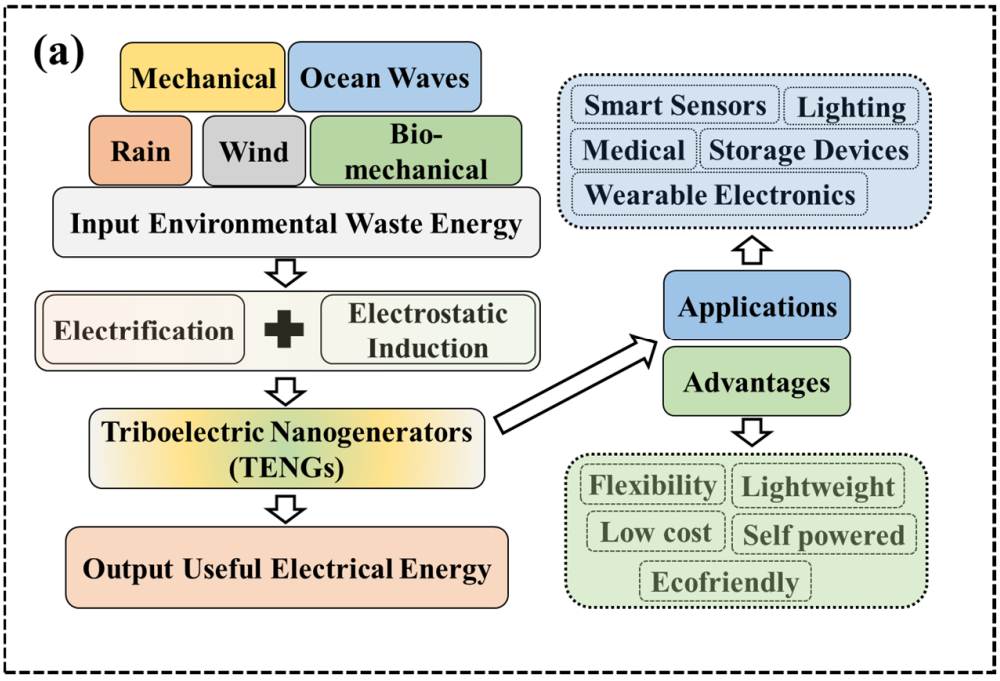


Figure 1. *Cont.*

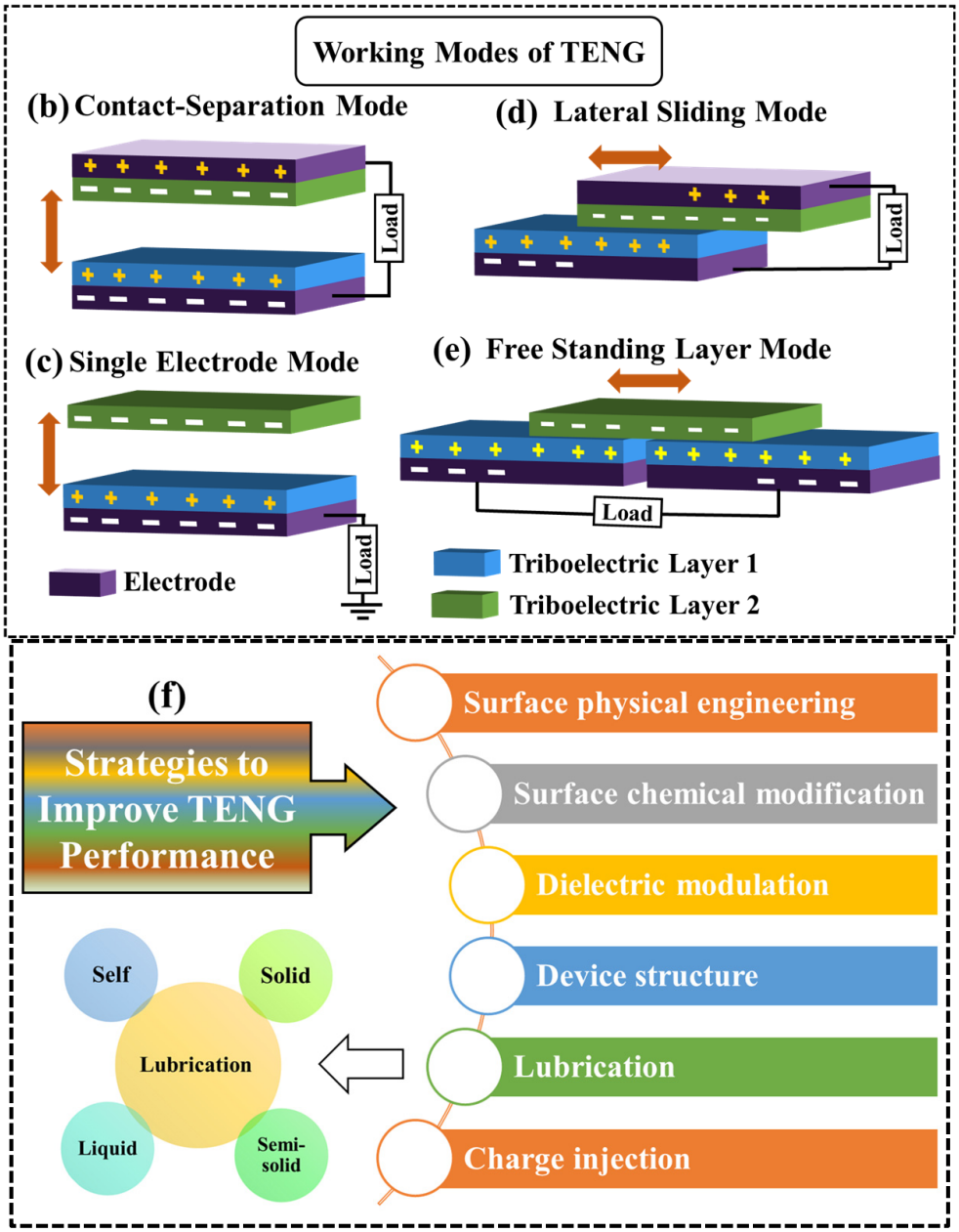


Figure 1. (**a**) An overview of TENG applications and advantages. The fundamental modes of TENGs: (**b**) Contact–separation mode. (**c**) Single-electrode mode. (**d**) Lateral-sliding mode. (**e**) Freestanding layer mode [23–25]. (**f**) Strategies to improve TENG performance.

Triboelectric nanogenerators (TENGs) are categorized into four fundamental working modes: contact–separation (CS) [10,23–26], single-electrode (SE) [10,27,28], lateral-sliding (LS) [10,29,30], and freestanding layer (FS) [10,31,32] modes. In both CS and SE configurations, electrical output is generated through repetitive contact and separation between triboelectric layers [10,23,25]. In contrast, LS and FS modes operate via periodic sliding at the interface of triboelectric materials [10,24,25]. Despite differences in mechanical motion and structural design, all TENG modes are governed by the same underlying principles, contact electrification/triboelectrification, followed by electrostatic induction [10,33–35]. These configurations are engineered to harvest mechanical energy from diverse sources, such as wind [36], ocean waves [37], and human motion [38]. CS and SE modes rely on vertical contact–separation mechanisms, while LS and FS modes utilize lateral frictional

sliding to induce charge transfer [23,24]. A schematic illustration of these four TENG modes is presented in Figure 1b–e and briefly discussed in the following sections.

1.1. Contact–Separation Mode (CS)

Figure 1b depicts the contact–separation mode TENG (CS-TENG), known as the fundamental mode of the TENG. It comprises two triboelectric layers with differing electrical charges (positive and negative) that are separated by an air gap. These triboelectric materials are fixed to conductive electrodes, which together form the lower and upper parts of the TENG. The electrodes are connected to each other by an external electrical circuit [10,23,24].

In the contact–separation mode of TENGs, alternating current is generated through the repeated contact and separation of two triboelectric materials with opposite electrical charges [10,23,25,39]. The materials are arranged in a stacked configuration, and when an external mechanical force brings them into contact, charge transfer occurs across the interface, inducing positive and negative charges on the respective surfaces [10,23,25,26]. Upon release, the materials separate, forming an air gap that creates an electrostatic potential difference between the electrodes. This potential drives electron flow through the external circuit until equilibrium is reached. When the materials are pressed together again, the potential difference decreases, causing the electron flow to reverse direction. Through this cyclic process of contact and separation, alternating current is produced [10,23–25]. Initially, the triboelectric layers are uncharged and separated by an air gap, but repeated mechanical loading and unloading sustain the charge transfer and current generation. This mode offers several advantages for practical applications, including a simple structural design, high power density, and efficient energy harvesting at low frequencies [10,23–25].

1.2. Single-Electrode Mode (SE)

The single-electrode mode TENG (SE-TENG) stands out from the other modes due to its unique configuration, featuring just one triboelectric material, as illustrated in Figure 1c [23,24]. The SE-TENG consists of a single triboelectric material fixed on a conductive electrode, which is externally connected to the ground. In its initial position, the freely moving triboelectric material is away from the fixed material, resulting in no surface charges on the triboelectric material [23,24]. When the freely moving material encounters the fixed material, positive and negative charges are produced on opposite surfaces [10,23–25]. In this state, there is no flow of electrons through the electrical circuit. As the free material moves away, electrons flow from the electrode to the ground due to electrostatic induction, generating an electric signal. Following this, an equilibrium state of charges is reached. When the free material contacts the fixed triboelectric material again, the flow of electrons reverses, flowing from the ground to the electrode. Thus, the freely moving material alternately contacts and separates from the stationary material, facilitating the periodic exchange of electrons between the electrode and ground. This mechanism effectively generates alternating current within the electrical circuit [10,16,23–25,33].

1.3. Lateral-Sliding Mode (LS)

The lateral-sliding mode TENG (LS-TENG), illustrated in Figure 1d, operates on a principle similar to the CS-TENG but with a distinct mechanical motion. It consists of two triboelectric layers attached to two conductive electrodes and connected to an external circuit [23,24]. Initially, the layers are separated and uncharged; however, upon contact, the triboelectric effect induces equal and opposite charges on their surfaces [10,23–25]. Unlike CS-TENGs, the layers then slide tangentially under external force, causing the interfacial contact area to change. This lateral displacement separates the charges, creating a potential difference that drives electron flow through the circuit until equilibrium is reached. When the sliding layer returns to its original position, the potential difference decreases, and the

electron flow reverses, thereby generating alternating current through repeated forward and backward sliding [10,23–25]. Compared to CS-TENGs, LS-TENGs offer higher efficiency in charge generation due to continuous relative sliding rather than discrete contact, making them particularly advantageous for high-frequency energy harvesting applications [10,23–25].

1.4. Freestanding-Layer Mode

The freestanding-layer mode TENG (FS-TENG), illustrated in Figure 1e, consists of two triboelectric materials fixed onto separate conductive electrodes positioned on the left and right sides, with a freestanding triboelectric layer sliding freely over them [23,24]. When the top layer contacts the bottom surfaces, triboelectrification occurs, inducing equal and opposite charges on the respective materials [10,23–25]. The bottom surfaces retain stationary negative charges, while the positively charged top surface drives charge flow through the external circuit. As the top layer slides laterally, the overlap with the bottom electrodes changes, creating a potential difference that causes electrons to drift between the electrodes [23,24]. When the top surface overlaps with the left electrode, negative charges accumulate there; as it slides to the right, electrons flow toward the right electrode, generating a forward current. Conversely, when the top layer moves back leftward, the electron flow reverses, producing alternating current (AC) [10,23–25]. Thus, the repeated forward and backward sliding of the freestanding layer induces cyclic charge transfer through triboelectrification and electrostatic induction. This configuration is particularly effective for harvesting mechanical energy, as the sliding motion continuously generates alternating electron flow between the bottom electrodes [10,23–25].

As discussed in earlier sections, the basic requirements of a TENG are triboelectric materials, conductors, and external periodic mechanical excitation for operation [10,23–25]. Accordingly, its output performance depends on the choice of triboelectric materials, the dielectric properties of those materials, the applied external mechanical force, environmental conditions, surface morphology, and surface charge density [2]. Since these factors play an important role in the performance of TENGs, significant focus has been given to these factors to improve the performance of TENGs. Although TENGs offer advantages and potential applications, they still face several ongoing challenges, such as low electrical output and efficiency, as well as weak durability and robustness, delaying their journey towards real-time practical applications [40,41]. To improve the overall performance of TENGs, various cutting-edge techniques have been explored (Figure 1f), including optimization of device structures [42], development of new composite materials [42], alteration of the topography of material surfaces [43], chemical modification of material surfaces [43], lubrication of contact interfaces [44], dielectric modulation [42], and surface charge enhancement [41].

The sliding-mode TENGs, among the four modes of TENGs, have attracted substantial attention due to their capability to achieve higher charge density and superior energy collection efficiency [45,46]. This mode is distinguished by its generation of electric current through the relative sliding motion of triboelectric layers. Since these modes rely on the relative sliding of surfaces under external mechanical forces, friction inevitably arises at the contact interface. Consequently, the frictional performance of the triboelectric layers at the contact interface decides the short-circuit current, open-circuit voltage, durability, and energy conversion efficiency of TENGs [29–32,47–50]. Furthermore, the performance of TENGs is strongly influenced by the working environment. Air breakdown in dry conditions leads to a decrease in the electrical output, while friction-induced wear of triboelectric layers significantly reduces durability. These factors limit the effectiveness of TENGs in long-term energy harvesting and hinder their broader practical applications [49,51–55].

Lubrication is a long-standing practice that has been extensively used in tribology to reduce the friction and wear, thereby enhancing the lifetime and reliability of machin-

ery in automobile, aerospace systems, and nuclear power plants [56–59]. Likewise, by applying the lubrication strategy to the TENGs, the aforementioned challenges have been addressed [24,29–31,44]. Lubricants are solid, semisolid and liquid or nanomaterial additives dispersed in a liquid that essentially avoids the direct contact between surfaces under friction by forming a thin lubricating film. This film effectively reduces the friction and wear, thereby enhancing the durability and performance of mechanical systems [60,61]. In addition, liquid lubricants have a higher breakdown voltage (10–15 kV/mm) than that of air (3 kV/mm), which helps to improve the surface charges [62–64]. Taking advantage of lubricant, researchers have increasingly focused on lubricated TENGs to achieve enhanced output power, durability, and ensure reliable practical applications [29–31,44].

Previously, several reviews have demonstrated the fundamental theory [45], progress of TENGs [65], and techniques [42] to improve TENG performance. Reviews based on various materials, such as MXenes [66], oxides [67], polymers [68], two-dimensional (2D) materials [22], magnetic materials [69], and crystalline porous materials (CPM) [70] for TENGs, have been reported. Several reviews have also summarized TENGs based on papers [71], sport activities [72], electrospun nanofibers [2], textiles [25], and biowaste [73]. Ocean wave energy [74], wind energy [75], and other environmental energy [75] harvesting TENGs were summarized in a review published in the year 2020. Self-powered motion detection and marine applications of TENGs have been studied by H. Jiang et al. [76] and T. M. Dip et al. [77], respectively. Reviews on direct current (DC)-TENGs and power management technologies for TENGs were also reported previously [78,79].

Recent review articles provide only a general overview of lubricant-based TENGs, focusing primarily on electrical output and mechanical lifespan [44,51]. In contrast, our present review offers a systematic and comprehensive investigation of lubricant-based TENGs. It examines in detail the construction of lubricant-based TENGs, the roles of solid, semisolid, and liquid lubricants, and the influence of normal load and operating frequency, as well as the effects of lubricant volume concentration and mass fraction of triboelectric materials on the device performance. It also analyzes the tribological and triboelectrical performance of TENGs operating under various polar and nonpolar liquid lubricants, along with dry friction conditions. Furthermore, we present a comprehensive summary of quantitative data on friction coefficient, open-circuit voltage, and short-circuit current for both lubricant- and non-lubricant-based TENGs, which was not addressed in the previous reviews. Following this, the long-term stability and working mechanism of lubricated TENGs are discussed. In addition, an innovative, unique strain-induced electrification nanogenerator (SIE-NG), which is contact–separation free and frictionless, was discussed for low-frequency energy harvesting, offering superior power density and durability. This review highlights the real-time practical demonstrations of TENG applications, such as illumination of LEDs and bulbs, charging capacitors and batteries, powering a hygrothermograph, and assessment sport activities. These findings emphasize the potential of lubricant-based TENGs for reliable energy harvesting and diverse real-world applications. Overall, our manuscript provides timely advancements and the current status of lubricant-based TENG technology, offering a thorough overview of lubricant-based TENGs, accompanied by an extensive discussion of all their possible applications.

2. TENGs Based on Lubricants

Friction is inevitable in sliding-mode TENGs, as the triboelectric materials slide against each other under external mechanical force, resulting in friction at the contact interface. Most of the time, polymers have been preferred as triboelectric material due to their superior dielectric properties, low-cost, lightweight, and mechanical flexibility. Among the several polymers, Kapton, polytetrafluoroethylene (PTFE), and fluorinated ethylene

propylene (FEP) are always given priority in TENG construction due to their excellent charge retention capability [80]. However, due to the smaller thickness of polymer films, they experience severe wear under external mechanical force during dry sliding, and hence, the TENG device fails to achieve a high, as well as long-term, electrical output. Therefore, researchers have been focusing on the use of various lubricants to ensure high electric output and durability of TENGs [13,29,31,32,81].

2.1. Solid Lubricant-Based TENGs

Solid lubricants help to reduce friction and enhance wear resistance, thus providing protection for materials sliding relative to each other. In TENGs, solid lubricants are used to lower friction, protect the tribomaterials from wear damage, and enhance energy conversion [81,82].

Figure 2a illustrates the structural configuration of the cTENG, which consists of two concentric cylinders capable of sliding relative to each other. The device operates on the principle of sliding triboelectrification at the interface. A tightly wrapped case around the outer cylinder enables coaxial one-dimensional motion between the two cylindrical structures [81]. Polyimide film (Kapton) was selected as both the electrification material and supporting substrate due to its excellent triboelectric properties and high tensile strength, ensuring efficient electricity generation and durability. Copper stripes, 2 mm in width and deposited with a linear pitch of 4 mm, were patterned on both sides of the Kapton film. The electrode designs on opposite sides were shifted by half a pitch, making them complementary (Figure 2a(i,iii)). Two Kapton films with identical electrode patterns were then assembled to form a pair of contact surfaces (Figure 2a(ii)) [81].

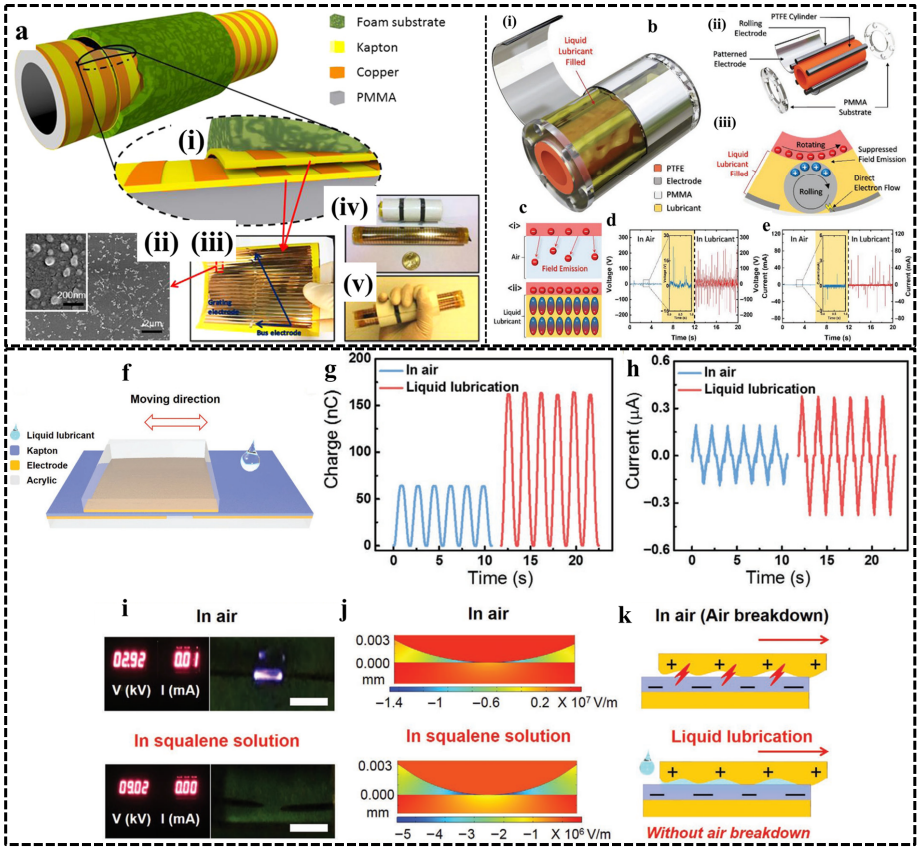


Figure 2. A case-encapsulated triboelectric nanogenerator (cTENG). (**a**) A 3D model of the cTENG and (**a**(**i**)) a cross-section view. (**ii**) An SEM image with different scales showing PTFE particles spread

on the surface of the Kapton. (**iii**) The Kapton film deposited with a grating copper electrode on both sides. A cTENG is shown (**iv**) before and (**v**) after assembly, with a 1 U.S. dollar coin as reference. Reprinted with permission from ref. [81], Copyright (2014), American Chemical Society. A schematic of LLS-TENG and the generated electrical output. (**b**(**i**)) A schematic (**ii**) construction and (**iii**) liquid lubricant filled state of LLS-TENG, (**c**(**i**)) air breakdown, (**c**(**ii**)) the suppression of field emission in liquid lubricant, (**d**) Voc, and (**e**) Icc output of the LLS-TENG in air and in lubricant conditions. Reprinted with permission from ref. [83], Copyright (2021), Wiley. The improved output performance of the sliding FS-TENG achieved through suppressing interfacial breakdown via interface liquid lubrication. (**f**) A structural schematic of the sliding FS-TENG with interface liquid lubrication. (**g**) Transferred charge, and (**h**) the short-circuit current of the sliding FS-TENG in air and with interface liquid lubrication. (**i**) Practical pictures of breakdown between two electrodes in air at 2.9 kV and without breakdown in liquid lubricant solution at 9 kV (scale bar, 0.4 cm). (**j**) A finite-element simulation of the electric field distribution in the micro gap between the triboelectric electrode and dielectric film in an air atmosphere or liquid lubricant solution (the surface charge density of each FEP film was 50 μCm^{-2}). (**k**) A schematic of interfacial breakdown in air and avoiding interface breakdown through interface liquid lubrication during sliding motion. Reprinted with permission from ref. [62], Copyright (2020), Wiley.

All copper stripes on the contact surfaces were interconnected by bus electrodes to create a common inner electrode (IE), while those on the back surfaces of the Kapton films served as the outer electrode (OE) (Figure 2a(iii)). To reduce friction and enhance energy conversion efficiency, spherical polytetrafluoroethylene (PTFE) nanoparticles were dispersed between the contact surfaces, as a solid lubricant (Figure 2a(ii)). The prepared Kapton films with electrodes were subsequently mounted on the outer surface of a poly (methyl methacrylate) PMMA tube and the inner surface of a foam tube, respectively (Figure 2a(iv)). The fully assembled cTENG is presented in Figure 2a(v) [81]. The fully constructed cTENG exhibited a maximum open-circuit voltage (Voc) of ~119 V and a short-circuit current (Isc) of 668 μA at a sliding velocity of 1.0 m/s. The instantaneous power and power density of the cTENG were 12.2 mW and 1.36 W/m^2, respectively, at a load of 140 kΩ [81].

The oleic acid-enhanced triboelectric nanogenerator (OA-TENG) was developed by Zhang et al. [82] using OA-doped polystyrene (PS), copper, nylon-11, and PI materials operating in the contact–separation mode. The OA-TENG exhibits a maximum Voc of 355 V, Isc of 9.4 μA, and a charge output of 44.55 nC at 4.8% OA doping in PS. Accordingly, the OA-TENG device achieves a maximum output power of 470.5 μW at a load resistance of 30 MΩ, which is much higher than that without OA doping (6 μW) [82]. The improved electrical performance and wear resistance of the OA-TENG are attributed to the OA, which enhances the electronegativity of PS and acts as a lubricating additive to reduce the friction and wear [82].

2.2. Semisolid Lubricant-Based TENGs

Greases are broadly utilized in many industries, such as machinery, automotive, food, steel, and textiles, owing to their capability to decrease friction and wear between moving parts [84,85]. Various greases, such as silicone, PTFE, fluorosilicone, and lithium grease, are classified as semisolid lubricants. They are applied at the contact interface of TENGs to reduce friction, mass loss, and wear, while simultaneously enhancing performance [32]. Accordingly, Zhao et al. [32] developed a grease-lubricated rotary freestanding TENG (RF-TENG) using copper and polymer as the triboelectric layers. The device consists of a stator and a rotator. The stator is composed of a copper electrode layer, a polymer layer fixed on the copper electrode, and an underlying substrate laminated along the vertical direction. The rotator is a copper electrode of radially arrayed sectors separated by equal-degree intervals [32]. The polymer layers tested in the study included PTFE, polyimide

(PI), and FEP film, along with different grease materials, such as PTFE, silicon, lithium, and fluorosilicone grease [32].

The friction and electrical output of the RF-TENG were first evaluated using a copper–PTFE pair in the presence of different greases over time. The RF-TENG initially exhibited increasing values of Voc and Isc, reached maximum levels, and subsequently decreased with further increase in time [32]. The peak-to-peak value of Voc in the RF-TENG under dry friction increased suddenly from 75.2 V to 103.9 V within a short period of 18 min. Subsequently, it decreased gradually by 76% and reached the stable Voc of 28.9 V at 180 min [32]. The decreased output over time is attributed to the formation of a transfer film on the copper electrode surface by the worn polymer [32].

The RF-TENG, based on the copper–PTFE pair with silicon and PTFE grease lubrication, exhibited enhanced electrical output and improved durability compared to the dry TENG. The silicone and PTFE grease lubricated RF-TENGs achieved maximum Voc values of 178.7 V and 151.6 V, respectively, within the initial 18 min. Thereafter, the values decreased by 20% and 18.7% at 180 min compared to their initial maximum values [32]. Lithium and fluorosilicone grease-lubricated RF-TENGs exhibited poor electrical performance compared to the dry TENGs. Among the tested grease lubricants, silicone showed the highest electrical output performance. The output was enhanced by 3.5 times compared to that of the dry TENGs. Likewise, the Isc of the TENGs under dry and grease lubrication showed a variation similar to that in the output voltage. It initially increased and then stabilized after a few minutes of testing. The silicone and PTFE lubricated RF-TENGs achieved maximum Isc of ~150 μA and ~140 μA, respectively, whereas the dry RF-TENGs generated only ~32 μA [32].

The average COF of RT-TENGs in dry, silicon, PTFE, fluorosilicone, and lithium grease lubrication was approximately 0.16, 0.12, 0.10, 0.11, and 0.14, respectively [32]. The electrical performance of the RF-TENGs based on copper–FEP and copper–PI was also studied under both dry and grease lubrication conditions. Both of the TENGs showed improved electrical output with silicon grease lubrication compared to the dry TENGs. However, the copper–PTFE pair demonstrated the superior electrical output and conversion efficiency [32].

Song et al. [86] developed a semisolid-lubricant-based ball-bearing type TENG, using steel balls, PTFE balls, aluminum electrodes, rotating substrates, and a semisolid lubricant (Super Lube). The ball-bearing TENG achieved a Voc of ~40 V and Icc in the range of 4–6 mA at a rotation speed of 100 rpm [86]. The ball-bearing TENG, consisting of three steel balls and three PTFE balls, exhibited an average peak voltage and current of 35 V and 1 mA at a load resistance of 1 MΩ, respectively. The corresponding output power of the device was 35 mW [86].

Zhao et al. [87] fabricated a grease-lubricated rotary freestanding TENG (GL-TENG), which consists of a stator and a rotator. The stator is composed of a PTFE layer attached to the stationary copper electrode and an underlying substrate. The rotator comprises a collection of radially arrayed sectors separated by equal-degree intervals [87]. The tribological and electrical performance of the TENG was evaluated under dry friction, as well as several grease lubrication conditions, such as electrical insulating grease, fluorosilicone grease, lithium-based grease, and PTFE grease [87]. Among these grease lubricants, insulating and PTFE grease have shown an enhanced voltage output, with insulating grease providing a higher output than PTFE grease. Accordingly, the rotary freestanding TENG under insulating grease lubrication achieved a maximum stable voltage of ~143 V, which is much higher than the 28.9 V obtained under dry friction. This improvement in voltage output with insulating grease can be ascribed to the suppression of air breakdown. The insulating grease enhances the breakdown field between the micro-gaps of the two triboelectric layers

in contact [87]. The friction coefficients of TENGs without grease lubricants were relatively high, with a value of ~0.12, whereas the grease-lubricated TENGs exhibited a range of 0.07–0.10. Specifically, the insulating grease-lubricated TENG showed a COF of ~0.09 [87].

The grease-lubricated triboelectric instantaneous angular speed sensor (GL-TEIASS) is integrated with a rolling bearing [87]. The electrical output characteristics of the GL-TEIASS and the sensor operating under dry friction (DF-TEIASS) were tested on the bearing-rotor test platform at a motor speed of 1000 rpm, a radial load of 200 N, and continuous running for 180 min [87]. The voltage of the GL-TEIASS was ~65 V, which is 4.1 times higher than that of DF-TEIASS. The current of the GL-TEIASS was ~65 μA, which is ~4 times higher than that of the DF-TEIASS. The power output of the GL-TEIASS was ~440 μW at a load resistance of 10 MΩ [87].

2.3. Liquid Lubricant-Based TENGs

Liquid lubricants play a vital role in mitigating the intrinsic limitations of TENG performance under dry friction, specifically by decreasing degradation of tribomaterials caused by wear, and suppressing the electric failure linked with air breakdown [13,29,83]. Liquid lubricants include silicon oil, paraffin oil, squalane, castor oil, water, ethyl alcohol, and mineral oil [13,29,31,83]. Under liquid lubrication, the electrical and tribological performance of TENGs is significantly improved through friction reduction, enhanced wear resistance, and suppression of air breakdown.

He et al. [13] projected a liquid lubrication-promoted sliding-mode TENG to overcome the challenges of the air breakdown and poor lifetime in conventional TENGs. Accordingly, a liquid lubrication-promoted TENG (LP-TENG), integrated with a voltage balance (VB) bar, was designed using nylon and PTFE triboelectric materials. The use of liquid lubricant in the TENG reduces material abrasion and enhances breakdown strength, further improving charge density and durability [13]. The measured charge densities of the traditional sliding-mode TENG operating in air and the LP-TENG operating in silicone oil were 0.626 $mC \cdot m^{-2}$ and 1.96 $mC \cdot m^{-2}$, respectively. The charge density of the LP-TENG is 216% higher than that of traditional TENGs. Further, the maximum peak power density of the LP-TENG in silicon oil was 4.43 $W \cdot m^{-2} \cdot Hz^{-1}$ at a load resistance of 100 MΩ [13]. A rotational LP-TENG prepared with a nylon and PTFE tribolayer operates under low-frequency mechanical energy. It achieves an open-circuit voltage above 20 kV at 60 rpm, whereas a maximum charge transfer of 2.0 mCm^{-2} was obtained at rotational speed within the range of 15–120 rpm. Further, the rotational LP-TENG exhibited average and peak power densities of 87.26 $Wm^{-2}Hz^{-1}$ and 562.36 $Wm^{-2}Hz^{-1}$, respectively, at an optimal load impedance of 80 MΩ [13].

The composite lubrication sliding-mode TENG (CL-STENG) was composed of a $BaTiO_3$ (BTO)/PI nanocomposite film, a copper metal electrode, and a PMMA substrate with various liquid lubricants. The BTO/PI film represents an excellent triboelectric material because of the combined effect of high wear-resistance from the PI matrix and the high dielectric constant from BTO. Both high wear resistance and high dielectric constant are essential to enhance the electrical output of TENGs [29]. The electrical output properties of the pure PI and BTO/PI nanocomposite film under various liquid lubricants (squalene, castor oil, and CD15W-40) were evaluated using the CL-STENG [29].

Among the tested liquid lubricants, squalane showed a higher steady-state Voc with both PI and BTO/PI films when used in the CL-STENG, whereas the output decreased under castor oil, even lower than that observed with dry frictions. No significant measurable output was obtained under CD15W-40 lubrication [29]. This behavior can be explained by the electrical conductivity of the lubricants; squalane has lower electrical conductivity than CD15W-40 and castor oil [29]. The triboelectric charges are neutralized under CD15W-40

and castor oil due to their higher electrical conductivity, leading to a decrease in the output. The conductivity of CD15W-40 is several orders higher than that of the others, resulting in no measurable output [29]. Under squalane lubrication, the triboelectric surface charges are barely neutralized because squalane has low electrical conductivity [29]. At the same time, squalene replaces air in the micro-gaps at the contact interfaces, which enhances the triboelectric charges generated by friction between the lubricant and solid material [29]. The steady-state Voc of BTO/PI (PI) under dry friction and squalane is ~38 V (~24 V) and ~165 V (~60 V), respectively. The higher performance of the CL-STENG based on the BTO/PI film with squalane lubrication arises from the synergistic effect between BTO and squalane [29]. Likewise, the average COF of CL-STENG based on PI and BTO/PI films under squalane lubrication is lower than that under dry friction. The average friction coefficient of PI (BTO/PI) under dry friction was ~0.36 (~0.42), and under squalane lubrication was 0.13 (~0.11). Other lubricants, such as castor oil and CD15W-40, exhibited lower COF compared to dry friction [29].

Chung et al. [31] developed a plate-type dielectric liquid-based self-operating switch triboelectric nanogenerator (DLSS–TENG), using dielectric liquid, aluminum electrodes, polystyrene (PS), and polytetrafluoroethylene (PTFE). The DLSS–TENG produced enhanced electrical output due to the dielectric liquid acting as an electrical switch to regulate air breakdown during operation [31]. When mineral oil was used as the dielectric liquid, the device demonstrated a maximum peak voltage of 140 V and an enhanced current of 30 mA under low-frequency mechanical excitation at 0.5 Hz. Furthermore, the DLSS–TENG was also operated with silicone oil, castor oil, water, and ethyl alcohol as lubricant media. Among these, mineral oil and silicone oil yielded the highest Voc and Isc values when employed as dielectric liquid media [31]. In addition, a disk-type DLSS–TENG was developed to continuously generate electricity by harvesting rotational energy from mechanical input. The materials used for the disk-type DLSS–TENG were similar to those of the plate-type device, including PTFE, aluminum, PS, and PMMA. Its electrical output was rectified using a diode. The disk-type DLSS–TENG exhibited a peak voltage of 100 V and a peak current of 56 mA at a rotational speed of 30 rpm in a mineral oil medium [31].

Chung et al. [83] developed a liquid-lubricant submerged TENG (LLS-TENG) to overcome the mechanical and electrical boundaries of conventional TENGs. As shown in Figure 2b, it is composed of a PTFE cylinder, aluminum rolling electrodes, aluminum plate electrodes, a PMMA cylinder substrate, and a liquid lubricant. The LLS-TENG was completely filled with liquid lubricant, as shown in Figure 2b(iii). Figure 2b(iii),c–e illustrates the enhanced current and voltage output of the LLS-TENG operated under liquid lubricant compared to TENGs in air [83]. When TENGs are not filled with liquid lubricant, the generated voltage and current are very low due to air breakdown. In contrast, because the breakdown voltage of liquid lubricant is higher than that of air, air breakdown is suppressed, resulting in higher voltage and current compared to TENGs operating under air. In addition, electrons in the rolling electrode flow directly to the plate electrode upon contact, enhancing the current output during rotation [83]. Thus, as shown in Figure 2d, the LLS-TENG exhibited a maximum Voc of ~200 V, which is higher than that of a TENG operating in air conditions (Voc $\approx$ 28 V). Likewise, the maximum closed-circuit current (Icc) of the LLS-TENG was 85 mA, compared to only 5 mA for a TENG in air, as shown in Figure 2e. In addition, the voltage, current, and power output of the LLS-TENG were evaluated across load resistance from 10 Ω to 1 GΩ at a rotation speed of 10 rpm. The instantaneous voltage was highest at 1 MΩ, while the current peaked at 10 Ω. Accordingly, the LLS-TENG achieved the maximum instantaneous power of ~0.6 W at a load resistance of 1 MΩ [83].

Zhou et al. [62] developed a sliding FS-TENG consisting of two conductive fabrics serving as a symmetric electrode, a Kapton film as an electrification layer, and a copper foil as a freestanding triboelectric layer, as shown in Figure 2f. Initially, a suitable liquid lubricant for TENG operation was identified by testing TENG in squalane, heptane, water, and alcohol. The results suggest that the TENG achieved a maximum transferred charge output of ~170 nC when operated in squalane [62]. The electrical output results of the FS-TENG operating at 10 N, with and without 50 μL squalane lubricant, are shown in Figure 2g,h. The lubricated FS-TENG showed a maximum transferred charge output of 160 nC and an Isc of 0.36 μA, which is approximately 2.5 times larger than that of the FS-TENG operating under air conditions [62]. The enhancement in electrical performance with squalane lubrication arises from the suppression of air breakdown, as illustrated in Figure 2i–k.

To establish a simple and effective approach for justifying air breakdown at the interface of triboelectric layers, Zhou et al. [62] studied the effect of squalane liquid lubricants, selected for their higher dielectric constant and low polarity compared to air [62]. The breakdown behavior of two electrodes in air and in liquid lubricant is shown in Figure 2i. At the same gap distance, no breakdown was observed in the liquid lubricant even at 9 kV, whereas a distinct breakdown happened at 2.9 kV under atmospheric conditions [62]. This reveals that breakdown is expressively more difficult to initiate in liquid lubricant than in air. Moreover, simulation results under identical contact states (Figure 2j) revealed that the electrostatic field strength within the micro gap between the triboelectric electrode and dielectric film decreases by an order of magnitude when air is replaced with liquid lubricant [62]. Collectively, these findings indicate that, relative to air, liquid lubricants suppress breakdown by increasing the required breakdown field strength and reducing the electrostatic field intensity in the micro gap. Consequently, electrostatic charge loss is greatly minimized, enabling improved charge accumulation on the triboelectric layers under the same contact conditions (Figure 2k) [62].

Mechanical energy from rotational motions, such as water flow and wind flow, can be conveniently harvested into electricity by rotary sliding TENGs, owing to their effective structural design [62]; however, their enduring stability remains challenging for practical use. This limitation could be overcome by adding liquid lubrication at the contact interface of the triboelectric layers [62]. Figure 3a illustrates the construction of the rotary sliding FS-TENG, which consists of a rotator and a stator, both designed with radially arrayed sectors. In this configuration, a Kapton film and a PCB board with a pre-deposited copper layer serve as the freestanding triboelectric layers, while conductive fabric is employed as the bottom electrode. To enhance performance, 100 μL of squalane was introduced at the triboelectric interface [62].

Furthermore, the peak power output of the lubricated rotary sliding FS-TENG was evaluated at a low operating frequency of 1.5 Hz under varying external load resistances. As shown in Figure 3b, the matched impedance decreased from 10 MΩ to 5 MΩ after liquid lubrication, indicating an increase in device capacitance [62]. In addition, the maximum power density rose from 1.24 to 3.45 $W \cdot m^{-2} \cdot Hz^{-1}$ (with peak power increasing from 21.7 to 32.9 mW), representing a three-fold improvement compared to previously reported rotary sliding FS-TENGs with shielding layers and alternative blank tribo-areas [62]. The suppression effect of liquid lubrication on electrostatic breakdown is further confirmed by examining the complementary electrode under open-circuit conditions. While significant breakdown phenomena were observed in the normal device, no breakdown occurred in the lubricated electrode, demonstrating the protective role of liquid lubrication [62].

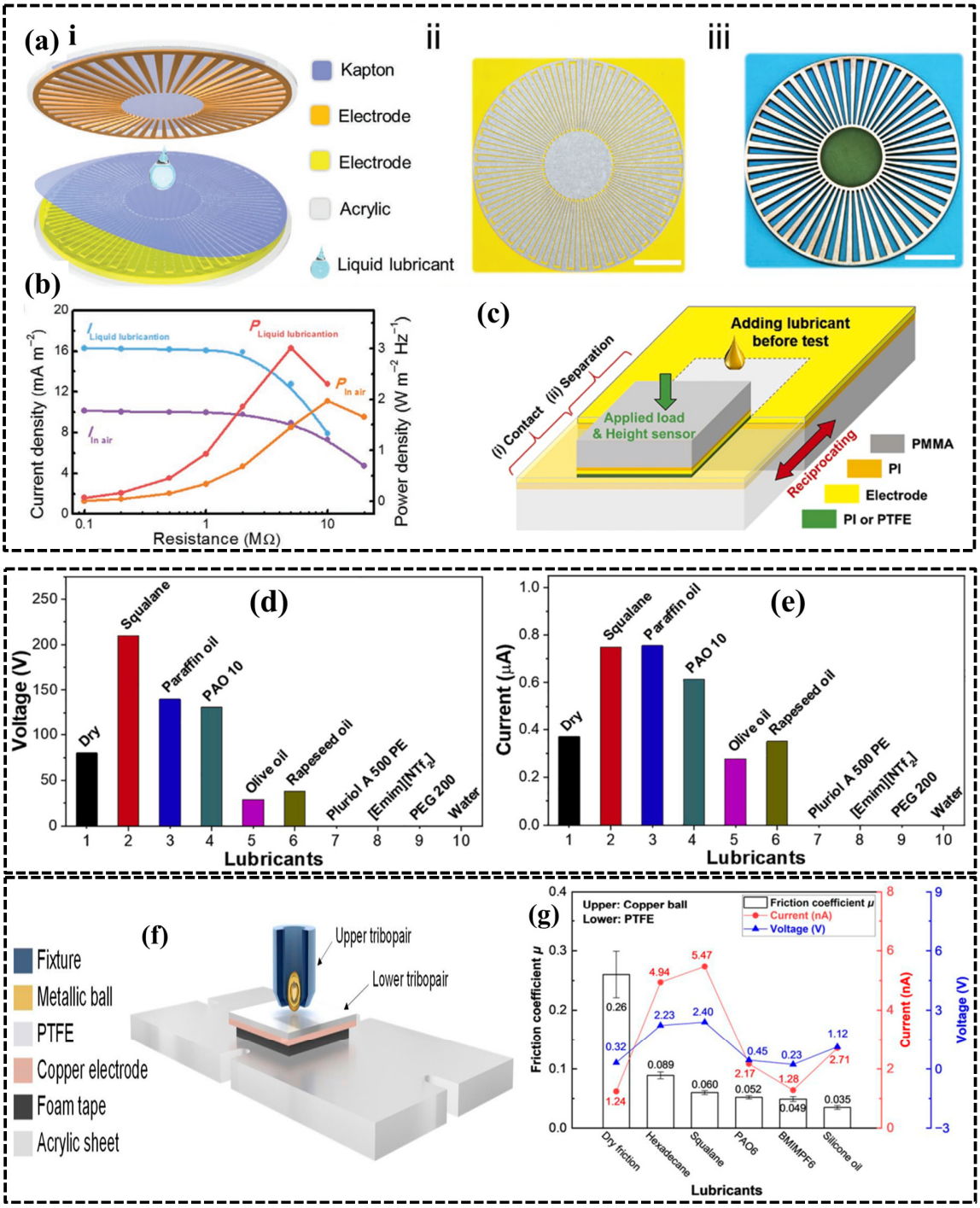


Figure 3. The Output performance of the rotary sliding FS-TENG via interface liquid lubrication. (**a**(**i**)) A schematic illustration of the rotary FS-TENG with interface liquid lubrication, (**ii**) photographs of the stator, and (**iii**) the rotator in the rotary FS-TENG (scale bar, 2 cm). (**b**) The output current density and power density of the rotary sliding FS-TENG with various resistances. Reprinted with permission from ref. [62], Copyright (2020), Wiley. A comparison of electric outputs between dry and liquid-lubricated TENGs. (**c**) A schematic diagram of the slide-mode TENG, (**d**) voltage, and (**e**) current for dry and different liquid-lubricated TENGs (Load—10 N). Reproduced from ref. [30], Copyright (2020), Elsevier. (**f**) A schematic diagram of the lower (PTFE) and upper (metallic ball) tribopair of the ball–plate configuration. Reproduced from ref. [88] under CC BY 4.0 license. Tribological and triboelectrical performances of the PTFE film–copper ball contact under dry friction and liquid lubrication conditions (Load—5 N, sliding speed—200 mm/s). (**g**) The average friction coefficient, maximum short-circuit current, and maximum open-circuit voltage. Reproduced from ref. [88] under CC BY 4.0 license.

Figure 3c shows the structure of the slide-mode TENG composed of PI and Al films. The slide-mode PI-Al TENG was employed to investigate the electrical and tribological performance under lubrication with different liquids, operating at an applied load of 10 N and frequency of 1 Hz. The comparative results are shown in Figure 3d,e. Notably, squalane-, paraffin oil-, and PAO10-lubricated TENGs exhibited enhanced voltage and current outputs, with squalane delivering the most significant improvement. In contrast, other liquids, such as Pluriol A 500 PE, PEG 200, [Emim][NTf_2] ionic liquid, and water, produced negligible electrical outputs [30].

The reciprocating-sliding TENG, based on perfluoroalkoxy alkane (PFA) polymer plate and aluminum electrodes, was operated under a normal force of 1 N and a frequency of 0.5 Hz with mineral oil, soybean oil, liquid paraffin, and silicone oil lubrication [89]. The device produced average peak voltages of 140, 142, 140, and 116 V under mineral oil, soybean oil, liquid paraffin, and silicone oil lubrication, respectively. Similarly, the average peak currents were 41.6, 37.6, 40, and 39.2 mA under mineral oil, soybean oil, liquid paraffin, and silicone oil lubrication, respectively [89].

The rotation-based TENG, composed of bottom aluminum and upper PFA plates with mineral oil liquid lubrication, was used to generate a continuous electric output by harvesting mechanical rotational energy. The rotation of upper PFA plates against the bottom aluminum plates continuously and simultaneously produced both long-duration and sharp peak outputs [89]. Accordingly, the sharp peak output and continuous long-duration peak output of the rotation-based TENG were 200 V and 2 V, respectively. Moreover, according to the surface photographs of the PFA plate, severe wear was observed after 24 h of working without lubrication, whereas the surface of the PFA remained relatively unworn under mineral oil lubrication, showing the improved tribological behavior of TENG when lubricated [89].

The hexadecane-containing sandwich structure-based TENG (HS-TENG) consisted of PTFE and nylon films as top and bottom triboelectric layers, respectively. Copper tape and hexadecane were used as the electrode and liquid lubricant, respectively. Hexadecane was sandwiched between PTFE and nylon film. The 10 N load was applied on the PTFE film, and a nylon film slid against the PTFE film with a velocity of 125 mm/s, producing electricity. The TENG without hexadecane produced a voltage of 19 V and a current of 6 μA. However, in TENG with hexadecane, hexadecane was spread on nylon using a brush, resulting in a hexadecane-containing sandwich structure, which generated 216% enhanced voltage and 150% enhanced current. The HS-TENG generated a voltage of 60 V and a current of 15 μA. The increased electrical output due to the formation of a hexadecane liquid film sandwiched between the PTFE and nylon films [90].

Furthermore, polyalphaolefin2 (PAO2), dodecane, PAO10, PAO6, paraffin oil, squalane, ethylene glycol, and 1-Butyl-3-methylimidazolium hexafluorophosphate (BMIMPF6) liquids were applied on nylon to form liquid-containing sandwich TENG structures. The TENGs containing paraffin oil, squalane, PAO6, PAO2, hexadecane, or dodecane oil film could all generate 32~230% enhanced voltage, while 12~98% reduction in voltage was observed for ethylene glycol, BMIMPF6, and PAO10. Among these liquids, hexadecane showed excellent electrical output by increasing the voltage by 230% and power by 10 times compared to the TENGs without liquid [90].

The lateral sliding TENG (LS-TENG), based on the charge excitation (CE) approach, referred to as CE-LS-TENG, consisted of the LS-TENG and the charge excitation approach. The LS-TENG comprised a top copper electrode, a middle PI film, and a bottom copper electrode [91]. The CE approach was executed by applying a pump voltage across the two ends of the LS-TENG. The device used to apply the pump voltage was composed of bottom and top acrylic substrates, a top copper electrode, and a packaging material [91].

The experimental outcomes of the CE-LS-TENG indicate that its tribological performance is improved by the enhanced coverage of the transfer film obtained through pump voltage [91]. However, the electrical properties of the CE-LS-TENG are limited by the increased transfer film coverage under the influence of pump voltage, resulting in the electrical output improving only within a specific range of pump voltage [91].

Squalane, a nonpolar liquid lubricant, was introduced between the contact surfaces of triboelectric materials to mitigate the limitations associated with transfer film formation, suppress air breakdown, and prolong the lifespan of the CE-LS-TENG [91]. The time-lapse images captured during the dry friction and squalane lubrication conditions clearly indicate that air breakdown occurs at the edge of the CE-LS-TENG under dry friction, whereas no air breakdown is observed under squalane lubrication, confirming its suppression [91].

The CE-LS-TENG achieved a maximum electric output of approximately 40 nC with 200 μL of squalane, compared to about 13 nC under air. Similarly, the COF value of the CE-LS-TENG was ~0.64 under dry friction conditions with a pump voltage of 1100 V, which is higher than the COF of ~0.2 under liquid lubrication conditions. The output charge density of CE-LS-TENG was approximately 148 $\mu C/m^2$ under squalane lubrication, with a pumping voltage of 1100 V, whereas it was around 125 $\mu C/m^2$ without voltage and ~48 $\mu C/m^2$ under friction conditions with no voltage. Overall, squalane lubrication enhances both the electrical and tribological performance of the CE-LS-TENG compared to air conditions [91].

Friction and wear are critical factors that determine both the performance and lifetime of TENGs. Inspired by the design of cylindrical roller bearings, Wang et al. [92] developed an oil-enhanced rolling-friction TENG (ORF-TENG) that combines high output with reduced friction. The device was fabricated using PI film, hexadecane, and acrylonitrile butadiene styrene (ABS) rollers. The ORF-TENG achieved a maximum Voc of 1256.7 V and Isc of 5.14 μA. This enhanced output performance is attributed to the synergistic interaction between the rollers and hexadecane [92]. To further evaluate its electrical characteristics, the dependence of voltage and current output on load resistance was measured. As the load resistance increased from 10 to 1013 Ω, the output voltage rose from 5.125×10^{-5} V to 835.6 V, while the output current decreased from 4.36 μA to 0.02 μA. The instantaneous output power reached 1.14 mW [92].

2.4. Ball–Plate Type Liquid Lubricant-Based TENGs

The frictional process of metal–metal contact, or of materials relative sliding to each other, results in triboelectrification. Consequently, friction unavoidably occurs whenever materials in close mechanical contact slide against one another, thereby influencing triboelectrification. It is, therefore, important to measure friction and triboelectrification simultaneously in order to understand their correlation and further improve TENG performance [23,53,88,93,94]. In this section, ball-on-plate type TENG configurations with liquid lubrication are discussed.

Li et al. [53] investigated the triboelectrification behavior of a GCr15 steel ball and a cast-iron disk under both dry and oil lubrication conditions. The results demonstrated that the changing trends in the friction coefficient and triboelectric current were consistent during the friction process. Triboelectrification in the metal–metal contact pair, initially driven by material transfer, was closely related to the friction and wear conditions [53]. The more severe the wear, the larger the triboelectric current; conversely, the less severe the wear, the smaller the triboelectric current [53]. Accordingly, the amplitude of triboelectric current under oil-free lubrication is higher than that under oil lubrication [53].

Friction between materials subjected to sliding leads to triboelectrification; hence, Liu et al. [93] investigated triboelectrification using a ball-and-plate setup, which is com-

monly employed to measure friction. An integrated system with a ball-on-flat configuration was developed to simultaneously detect tribocurrent and friction coefficient [93]. A bearing steel ball (GCr15) and a polyvinylidene fluoride (PVDF) block were used as the friction pair. The triboelectric current generated during the friction process was collected through the steel ball, which was fixed in a copper fixture, clamped by an insulating acrylic rod, and connected to a current amplifier via copper wire. The friction coefficient was measured using a friction testing machine [93].

The steel ball and PVDF-based TENG with polyalphaolefin (PAO) base oil was operated at a frequency of 4 Hz, an applied load of 5 N, and a stroke length of 2 mm. The current and voltage generated during friction between the steel ball and PVDF in the presence of 0.5 μL PAO 4 were 6 nA and 0.15 V, respectively, which are higher than the current of 0.8 nA and voltage of 0.05 V produced under dry conditions [93]. The friction coefficient (COF) of the steel ball–PVDF TENG continuously increased and reached 0.17 after 200 s in the dry state, whereas it decreased to around 0.07 under PAO oil lubrication [93]. It was observed that the surface of the PVDF became rough due to wear, resulting in increased micro-gaps. During dry friction, tribocharges were lost through air breakdown when the steel ball encountered these micro-gaps [93]. In contrast, the addition of PAO lubricant at the contact interface of the friction pair displaced the air in the micro-gaps. Consequently, air breakdown at the contact interface was suppressed because the PAO liquid lubricant has a lower polarity and a higher dielectric constant than air [93]. Moreover, materials with high dielectric constants can retain more charges. The tribocharges were further enhanced as the PAO lubricant filled the micro-gaps where the steel ball and PVDF could not make direct contact [93].

Chen et al. [88] developed a ball-on-plate reciprocating-sliding testing platform capable of simultaneously measuring electrical output and friction coefficient. The sliding-mode TENG was composed of a metallic ball (copper or steel) and PTFE films, as shown in Figure 3f. To identify suitable liquid lubricants for reducing friction and enhancing triboelectrical performance, a series of liquid lubricants, including silicone oil, BMIMPF6, PAO6, squalane, and hexadecane, was evaluated by operating the TENG under these lubricants at a sliding speed of 200 mm/s and an applied load of 5 N [88]. The average COF and maximum Isc and Voc values for the copper ball–PTFE TENG under dry and different lubrication conditions are summarized in Figure 3g. The copper–PTFE TENG under dry friction exhibited a stable COF of 0.26 at 2400 s, following an initial fluctuating value, starting from 0.13. Interestingly, when operating with five liquid lubricants, the friction coefficients decreased to values below 0.10, with the lowest COF of 0.035 observed for silicon oil. The reduction in COF under liquid lubrication conditions can be attributed to the formation of a liquid film at the contact interface, which effectively reduces the friction [88].

The maximum Isc and Voc, under dry friction conditions, were 1.24 nA and 0.32 V, respectively. The triboelectric performance of the copper ball–PTFE TENGs was notably enhanced when lubricated with silicone oil, PAO6, squalane, and hexadecane, although the Voc slightly decreased to 0.23 V under BMIMPF6 lubrication [88]. The highest Isc of 5.47 nA and Voc of 2.40 V were achieved with squalane lubrication. In comparison, silicone oil lubrication increased the Isc and Voc by 2.2-fold and 3.5-fold, respectively, relative to the dry friction case [88]. Although the electrical performance was improved under liquid lubrication, the electric output varied significantly, depending on the dynamic viscosity and relative permittivity of the lubricants. In general, low viscosity and low permittivity are favorable for achieving superior electric performance [88]. Consequently, silicone oil lubrication yielded a stable, low COF of 0.035, along with an output Isc of 2.71 nA and

a Voc of 1.12 V, highlighting its strong potential for achieving outstanding triboelectric performance in PTFE films [88].

Shao et el [94] used a testing platform that simultaneously measures friction and triboelectric output generated during the contact between a steel ball and polymer films, including PDMS, PTFE, TPU, and PI. The experimental results with a sliding speed of 40 mm/s under a load of 5 N in dry conditions suggest that the Voc and Isc of the PTFE film are highest among the other polymer films, while the highest transferred charges are observed in PI films [94]. Because of the electron-withdrawing nature of the amide group, PI exhibits a strong capacity to attract electrons. This characteristic enables PI to effectively capture and retain charges during frictional contact. Although PTFE demonstrates superior performance in terms of voltage and current generation, its effective charge is significantly lower than that of PI, with a difference of about 0.4 nC. This reduction may be attributed to the dissipation of charges generated during friction through air or other surrounding media. The variation in triboelectric performance is closely associated with the interactions between the contacting surfaces during sliding, as well as their chemical composition [94]. The average COF in the steady state of four polymers, PDMS, PTFE, TPU, and PI, was 0.552, 0.135, 0.245, and 0.310, respectively.

The liquid superlubric TENG was constructed by Wang et al. [95] using a PTFE ball, an ITO-coated glass disc, and PAO lubricant with a viscosity of 3.98 mPa·s. The PTFE ball was secured to a force sensor via a fixture, while the glass disc was mounted on a rotating platform. A conductive sheet, relying on elastic deformation, maintained contact with the copper tape along the edge of the glass disc and was connected to the electrical measurement system through a conductive wire. Experimental conditions were set with a normal load of 15 N and a rotation speed of 300 rpm. The PTFE ball was positioned 10 mm from the rotational center of the glass disc, defining the rotation radius [95]. The electrical output performance of both the lubricant-free TENG and PAO lubricated superlubric TENG was evaluated. Compared with the lubricant-free TENG, the liquid superlubric TENG exhibited significant enhancements, with the typical Voc and Isc increasing by 155.6% and 140.5%, respectively, reaching 1.02 V and 100.9 nA [95].

The evolution of the COF for both devices was also monitored over time. For the lubricant-free TENG, the friction coefficient initially increased and then fluctuated within a narrow range, ultimately reaching 0.285 at the end of the test [95]. In contrast, the liquid superlubric TENG rapidly entered a highly stable superlubricity state under standard laboratory conditions without atmospheric control. Its COF started at 0.0088 and continued to decrease to 0.0025 after 127 min, representing a 99.1% reduction compared with the lubricant-free TENGs [95]. Traditionally, the electrical output of TENGs increases with higher friction. However, our findings demonstrate that the liquid superlubric TENG achieves more than a 100% increase in electrical output while simultaneously reducing friction by 99.1%, thereby operating in a superlubricity state [95].

The tribological behavior-controlled direct-current TENG (TCDC-TENG) was composed of steel balls and N-type Si-wafers coated with a thick Au film. Specifically, a ball-on-flat configuration (steel ball-on-Si wafer) was used to measure the tribological and triboelectrical characteristics of a steel ball reciprocating on the Si-wafer in order to establish a correlation between friction and charge generation at a metal–semiconductor contact [96].

Accordingly, the tribological and triboelectrical properties of the TCDC-TENG were evaluated under dry friction and with various liquid lubricants, including PAO4, PAO6, PAO10, mineral oil, ethylene glycol, hexadecane, and silicon oil. Initially, static and dynamic I-V curves of the TCDC-TENG with and without PAO4 lubrication were investigated. The results suggest that the steel ball–Si wafer heterojunction behaves as a Schottky contact under both dry friction and PAO4 lubrication, with a stronger rectified Schottky barrier

observed under PAO4 lubrication due to the presence of the lubricating oil film [96]. The TCDC-TENG showed an Isc of 0.517 nA and a DC output voltage of 0.65 V under dry friction, with a load resistance of 40 MΩ, an applied load of 5 N, and a sliding frequency of 5 Hz. However, when operated under PAO4 oil, the performance of the TCDC-TENG slightly decreased, with the DC output voltage reduced to 0.55 V and the Isc lowered to 246 nA under the same operating conditions. Among the tested lubricants, the PAO4 lubricated TCDC-TENG demonstrated a higher DC output voltage, while the others maintained a lower DC voltage output [96].

The tribological and triboelectric performance was simultaneously investigated by developing a freestanding-triboelectric-layer-mode TENG, based on 316 L steel and a PTFE sheet [97]. The performance was tested under dry, hexadecane, and hexadecane–OLC lubrication conditions, with an applied load of 5 N, a reciprocating stroke of 24 mm, and a frequency of 2 Hz. The maximum generated current during dry friction was only 70 nA; however, it increased to 130 nA and 400 nA in the presence of hexadecane and hexadecane–OLC lubrication, respectively. The output current under hexadecane–OLC increased by 5 and 2 times compared to that of dry and hexadecane lubrication conditions, respectively. Likewise, hexadecane–OLC lubrication showed enhanced charge transfer, which is nearly 7 times higher than dry conditions, and 2.2 times higher than under hexadecane lubrication [97]. Furthermore, the COF of the TENG under dry friction was 0.22, whereas it was much reduced to 0.054 and 0.048 after the addition of hexadecane and hexadecane–OLC lubricant, respectively. It was observed that during dry friction, the PTFE surface was severely worn; however, after the addition of lubricant, the wear was reduced compared to dry friction. The PTFE surface exhibited minimal wear under lubrication, and hence, its electrical output performance was better than under dry friction [97]. Several other liquid lubricants, including water, polyethylene glycol 200 (PEG 200), ethylene glycol (EG), and polyalphaolefin 6 (PAO 6), were tested to evaluate their effect on friction and electrical output. Among these, hexadecane–OLC gives the best electrical performance and the lowest friction coefficient, suggesting its superiority in TENG applications [97].

Rotating mechanical energy was harvested using a rotating wheel disk TENG composed of a PTFE–steel pair and lubricated with hexadecane–OLC, operating under a load of 18.6 N and a rotating speed of 300 rpm. A tribeoelctrical performance evaluation of the wheel TENG showed higher electrical output with hexadecane–OLC lubrication compared to hexadecane lubrication and dry conditions [97]. The wheel TENG showed only a 1.2 μA current output under dry conditions, whereas it produced 2.5 μA and 4 μA under hexadecane and hexadecane–OLC lubrication, respectively. Likewise, transferred charges, voltage, and power from the wheel TENG were higher with hexadecane–OLC lubrication compared to dry and hexadecane lubrication conditions. The maximum power of the wheel TENG was 225 μW under hexadecane–OLC lubrication [97].

2.5. Self-Lubrication-Based TENGs

Sliding-freestanding TENGs (SF-TENGs) were composed of DT, copper, and conductive fabric electrodes. Likewise, SF-TENGs were fabricated by replacing the DT with PT and PT/SiO_2. The electrical output performance of all these SF-TENGs is shown in Figure 4a–c, which were operated at an applied load of 5 N and frequency of 3 Hz [98]. A porous THV (PT) and dense THV (DT) are negative terpolymer tribo-materials comprising tetrafluoroethylene (TFE), hexafluoropropylene (HFP), and vinylidene fluoride (VDF). PT/SiO_2 refers to porous THV (PT) film modified with 0.5 wt.% oleophilic silicon dioxide nanoparticles (SiO_2) [98].

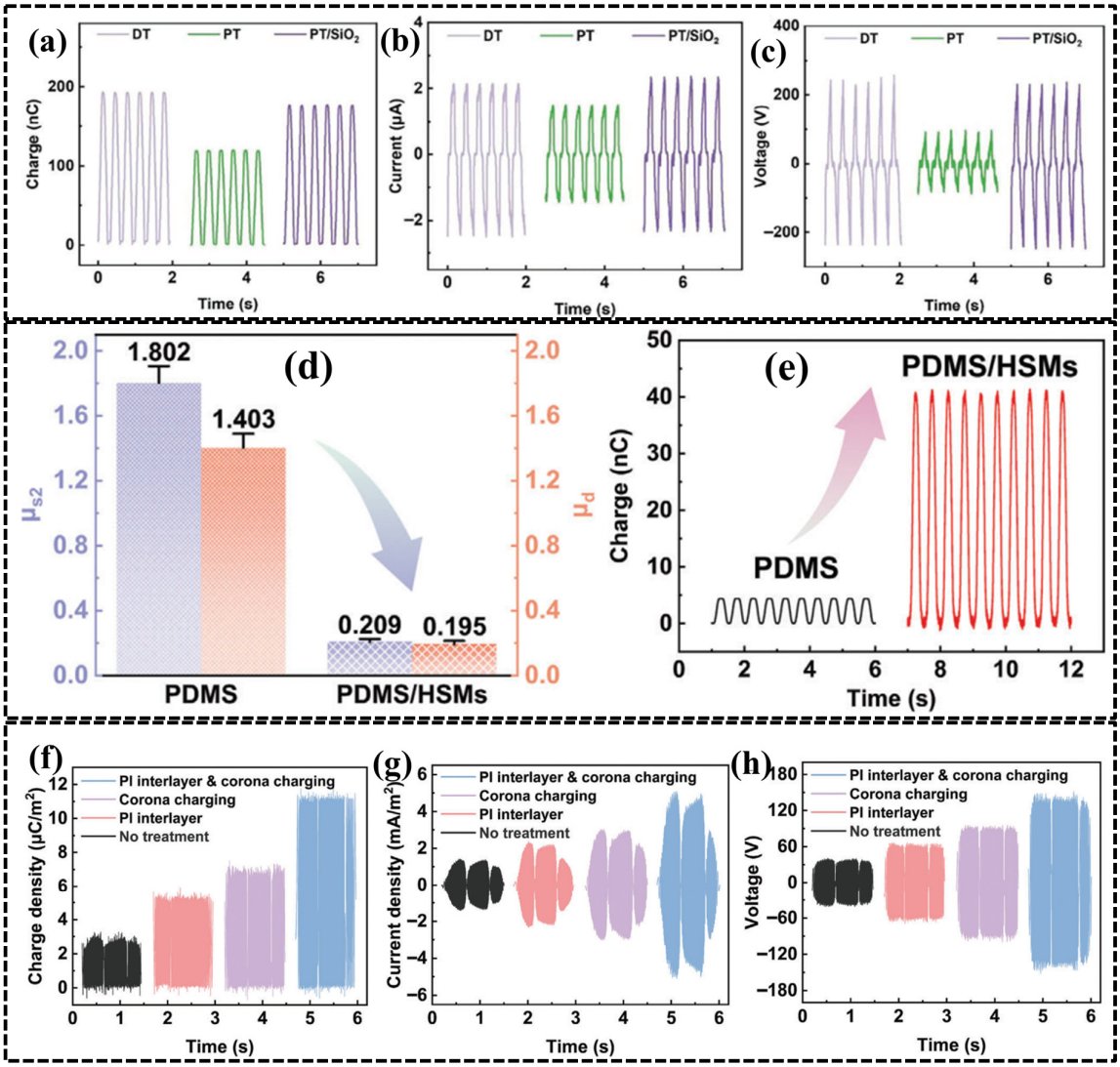


Figure 4. (**a**) Transferred charges, (**b**) short-circuit currents, and (**c**) output voltages of DT film, PT film, and PT/SiO_2 film in contact with Cu foil, respectively. Reproduced from ref. [98] under CC BY 4.0 license. The friction and charge output of the surface-textured self-lubricating PDMS/HSMs film. (**d**) Static and dynamic COFs obtained from the dynamic sliding friction test. (**e**) The transferred charges of the two SF-TENGs with the pristine PDMS film and surface-textured self-lubricating PDMS/HSMs film as the electronegative tribo-layer. Reprinted with permission from ref. [99], Copyright (2023), Wiley. The influences of the PI interlayer addition and corona charging treatment on the output performance of the prepared TAB-TENG. (**f**) Transferred charges, (**g**) short-circuit currents, and (**h**) output voltages of the four TAB-TENGs during a single excitation. Reprinted with permission from ref. [99], Copyright (2023), Wiley.

The electrical output of the PT film was lower than that of the DT film, confirming the diminished performance of PT compared to DT (Figure 4a–c). The PT film has a porous structure, which reduces the effective contact area; large pores cause charge dissipation and poor storage ability, while the decreased dielectric constant further lowers the electrical output [98]. Together, these factors reduce the overall performance of PT. However, this issue was addressed by modifying the PT film with the 0.5 wt.% SiO_2. As shown in Figure 4a–c, the electrical output of PT was improved by the incorporation of SiO_2, owing to improved dielectric constant and effective charge trapping capability of the SiO_2 nanoparticles [98].

A surface-textured PDMS/HSMs film with micro-bump surface topography was prepared by self-assembling hollow SiO_2 microspheres (HSMs) near the surface of a poly-

dimethylsiloxane (PDMS) film under vacuum conditions [99]. The static and dynamic sliding friction test results of PDMS-Cu and PDMS/HSMs-Cu pairs are shown in Figure 4d. The static and dynamic COF values of the PDMS-Cu pair were 1.802 and 1.403, respectively, while those of the PDMS/HSMs-Cu pair were 0.209 and 0.195, respectively. These results indicate that the as-prepared surface-textured PDMS/HSMs film possesses an ultra-low COF with self-lubricating properties, originating from its reduced surface elastic deformation and contact area [99].

The pristine PDMS film and the self-lubricating PDMS/HSMs film were used in the construction of a sliding-freestanding TENG (SF-TENG), in which both films act as negative triboelectric layers. Furthermore, the electrical performance of the TENG was evaluated under a reciprocating-sliding frequency of 2 Hz [99]. The transferred charge of the SF-TENG based on the PDMS/HSMs film was 40.9 nC, which is significantly higher than that of the PDMS film-based TENG (Figure 4e). Similarly, the SF-TENG consisting of PDMS/HSMs film showed markedly improved output with a current of 0.5 μA and a voltage of 48.8 V, compared to the PDMS-based TENG [99]. A micro-bump surface-textured PDMS/HSMs film represents a self-lubricating material with low COF, enhanced sliding stability, and improved contact intimacy, all of which collectively lead to a remarkable improvement in the contact electrification [99]. In addition, the excellent charge-trapping capability of the HSMs electret, interfacial polarization between the HSMs and PDMS molecular chains, and improved dielectric constant contribute to superior output performance [99].

A textured film and self-adapting contact-synergized bidirectional rotary TAB-TENG was introduced to harvest biomechanical energy using a surface-textured self-lubricating PDMS/HSMs film. In addition, a PI layer was incorporated as a charge-storage interlayer, while polyethylene terephthalate (PET) served as the mechanical support layer. Moreover, a corona charging approach was employed to increase surface charge density rapidly [99].

The four different TAB-TENGs were composed of: PI interlayer with corona charging, corona charging alone, PI interlayer alone, and no treatment, in order to evaluate the effects of corona charging and the charge-storage PI interlayer. The corresponding electrical outputs of the four TAB-TENGs are shown in Figure 4f–h [99]. The TAB-TENG, combined with PI interlayer and corona charging, achieved a maximum charge density of 11.4 μCm^{-2}, short-circuit current density of 5.1 mAm^{-2}, and an output voltage of 148 V (Figure 4f–h). Moreover, it demonstrated a peak current density, maximum peak power density, and maximum average power density of 2.9 mAm^{-2}, 274 mWm^{-2}, and 80 mWm^{-2}, respectively, which were obtained at a load resistance of 20 MΩ. Table 1 provides a summary of tribological and triboelectrical performance values of numerous TENGs working under dry as well as liquid/semisolid lubrication conditions. It contains the COF, voltage, current, power density, stability, and application demonstration of the TENGs, along with applied load and frequency.

Table 1. Summary of tribological and triboelectrical performance of lubrication-based TENGs.

TENG	Triboelectric and Electrode Materials	Lubricant	Load/ Frequency Velocity	COF	Voc	Isc	Power	Stability	Application	Ref.
Reciprocating and freestanding TENGs										
Lubrication-STENG	Copper and PI	Dry Squalane	16 N, 4 Hz	~0.36 ~0.13	~24 V ~60 V	-	-	−3.475 h	-	[29]
CL-STENG	Copper and BTO/PI film	Dry Squalene	16 N, 4 Hz	~0.42 ~0.12	~38 V ~165 V	-	-	3.475 h	-	[29]
Reciprocating Slide-Mode TENG	Al Foil and Kapton film (PI)	Dry Squalane	10 N, 1 Hz	-	~76 V ~215 V	~0.38 μA ~0.75 μA	-	36,000 cycles	-	[30]
Freestanding Reciprocating -Sliding DLSS-TENG	PTFE, PS, and Aluminum	Dielectric liquid Mineral oil	0.5 Hz	-	140 V	30 mA	-	-	LEDs lit	[31]
Sliding FS-TENG	Copper foil & Kapton, conductive fabric	Squalane	10 N	-	~450 V	0.36 μA	-	86% 500,000 cycles	-	[62]

Table 1. *Cont.*

TENG	Triboelectric and Electrode Materials	Lubricant	Load/ Frequency Velocity	COF	Voc	Isc	Power	Stability	Application	Ref.
Alternative Current TENG (AC-TENG)	Copper foil & Kapton, conductive fabric	Squalane	10 N	-	-	0.46 μA	-	500,000 cycles	-	[62]
DirectCurrent TENG (DC-TENG)	Copper foil and Kapton	Squalane	10 N	-	-	0.16 μA	-	500,000 cycles	-	[62]
Reciprocating-Sliding cTENG	Kapton and copper	PTFE nanoparticles	1.0 m/s	-	~119 V	668 μA	12.2 mW @ 140 kΩ	-	Green LEDs and white bulbs lit	[81]
Reciprocating TENG	PFA and Aluminum	Liquid paraffin Mineral oil	1 N, 0.5 Hz	-	140 V 140 V	40 mA 41.6 mA	-	-	-	[89]
HS-TENG	PTFE, Nylon, and copper tape	Dry Hexadecane	10 N, 125 mm/s	-	19 V 60 V	6 μA 15 μA	-	6000 s 64,000 s	-	[90]
CE-LS-TENG	Copper, and PI with CE, pump voltage 0 V	Dry Squalane	-	~0.47 ~0.13	-	~48 $\mu C/m^2$ ~125 $\mu C/m^2$ Charge density	-	12,000 s	-	[91]
CE-LS-TENG	Copper, and PI with CE, pump voltage 1100 V	Dry Squalane	-	~0.64 ~0.2	-	- ~148 $\mu C/m^2$ Charge density	-	12,000 s	-	[91]
Reciprocating-Freestanding TENG	316 L Steel and PTFE	Dry Hexadecane Hexadecane–OLC	5 N, 2 Hz	0.22 0.054 0.048	-	70 nA 130 nA 400 nA	-	-	-	[97]
ERB-SF-TENG	ERB film, copper, and conductive fabrics	Squalane	5 N, 3 Hz	0.077	277 V	2.78 μA	0.45 Wm^{-2} @304 MΩ	100,000 cycles	LED lightening, capacitor charging, LCD display	[98]
SF-TENG	Copper, PDMS/HSMs	Self-lubrication	2 Hz	0.195	48.8 V	0.5 μA	-	-	-	[99]
Ball–plate-type TENGs										
Reciprocating Ball–Plate	GCr15 and PVDF	Dry	5 N, 4 Hz	~0.15 @300 sec	0.05 V	0.8 nA	-	-	-	[93]
		PAO 4		~0.07	0.15 V	6 nA				
Reciprocating Ball–Plate	GCr15 and POM	Dry	5 N, 4 Hz	~0.15 @300 sec	-	0.5 nA	-	-	-	[93]
		PAO 4		~0.07	-	1.25 nA	-	-	-	
Reciprocating Ball–Plate	GCr15 and PTFE	Dry	5 N, 4 Hz	~0.15 @300 sec	-	0.25 nA				[93]
		PAO 4		~0.07	-	1.3 nA				
Ball-Plate Testing	PTFE and steel ball	Silicon oil 0.005 wt.% graphene NSs + Silicon oil	5 N, 200 mm/s	0.027 0.016	0.62 V 0.77 V	1.64 nA 2.14 nA	-	-	-	[88]
Ball-Plate Testing	PTFE and copper ball	Dry Hexadecane Squalane PAO6 BMIMPF6 Silicone oil	5 N, 200 mm/s	0.26 0.089 0.060 0.052 0.049 0.035	0.32 V 2.23 V 2.40 V 0.45 V 0.23 V 1.12 V	1.24 nA 4.94 nA 5.47 nA 2.17 nA 1.28 nA 2.71 nA	-	-	-	[88]
Reciprocating Ball-Plate	304 steel and PI	Dry Oleic acid (OA) 0.1 wt.% TiO_2 doped OA	5 N, 40 mm/s	0.310 0.022 0.066	~1.8 Vpp ~1.2 Vpp ~2.5 Vpp	0.7 nA ~0.6 nA ~1.25 nA	-	3600 s	-	[94]
Macroscopic Liquid Superlubric TENG	PTFE ball, ITO, and copper	Dry PAO	15 N, 300 rpm	0.285 0.0025	0.4 V 1.02 V	41.96 nA 100.9 nA	-	-	-	[95]
Reciprocating TCDC-TENG	Steel ball and Si-wafer	Dry PAO4	5 N, 5 Hz	~0.75 ~0.15	0.65 V 0.55 V	517 nA 246 nA	-	-	-	[96]
Rotating-sliding TENGs										
NFCL-TSS/Rotary Freestanding TENG (RF-TENG)	NUP2207 ECP Bearing Material, Cu, and BTO/PI film	Squalene	Radial load 200 N, 2500 RPM	-	80 V	~12 nA	-	2 h	Speed sensor	[29]
Rotating Disk-type DLSS-TENG	PTFE, PS, and Aluminum	Dielectric liquid Mineral oil	30 rpm	-	100 V	56 mA	-	-	Capacitor charging	[31]
Rotary Freestanding TENG (RF-TENG)	Cu & PTFE	Dry Silicon grease	12 N, Angular frequency-104.7 rad/s	~0.16 0.12	28.9 Vpp ~143 Vpp	~32 μA ~150 μA	-	-	-	[32]
Rotary Freestanding TENG (RF-TENG)	Cu & PI	Dry Silicon grease	12 N, Angular frequency-104.7 rad/s	~0.35 ~0.17	~42 V ~110 V	-	-	-	-	[32]

Table 1. *Cont.*

TENG	Triboelectric and Electrode Materials	Lubricant	Load/ Frequency Velocity	COF	Voc	Isc	Power	Stability	Application	Ref.
Rotary Freestanding TENG (RF-TENG)	Cu & FEP	Dry Silicon grease	12 N, Angular frequency-104.7 rad/s	~0.16 ~0.10	~40 V ~135 V	-	-	-	-	[32]
Rotary Sliding FS-TENG	Copper, Kapton film & conductive fabrics	Air Squalane	-	-	-	~115 μA ~150 μA	21.7 mW 32.9 mW	35% after 12,000 cycles 90% after 100,000 cycles	Lit up white LED bulbs, powering hygrothermograph	[62]
GL Rotary Freestanding TENG	Copper, PTFE, FR-4	Dry Insulating Grease	12 N, 1000 rpm	0.12 ~0.09	28.9 V ~143 V	-	-	-	-	[87]
GL-TEIASS	Copper, PTFE, FR-4	Dry Insulating Grease	Radial load 200 N, 1000 rpm	-	~15 V ~65 V	~15 μA ~65 μA	- ~440 μW @ 10 MΩ	-	Angular speed sensor	[87]
Rolling Freestanding LLS-TENG	PTFE and Aluminum	Air Mineral oil	-	-	28 V 200 V	5 mA 85 mA	-	72 h	319 LEDs, charging of capacitors and Li battery	[83]
Rotating TENG	PFA and Aluminum	Mineral oil	-	-	200 V	-	-	4000 s	Turn on 58 LEDs	[89]
Rotating Wheel Disc TENG	316 L steel and PTFE	Dry Hexadecane Hexadecane–OLC	18.6 N, 300 r/min	-	-	1.2 μA 2.5 μA 4 μA	~20 μW ~100 μW ~225 μW	30 min 30 min 6 h	50 LEDs lit	[97]
TAB-TENG	Copper, PDMS/HSMs, PI	Self-lubrication	6 N	-	148 V	5.1 mA m^{-2}	80 mWm^{-2} @20 MΩ	350,000 cycles	LED lightening, LCD blackboard display, walking monitoring	[99]
Bearing-type and rolling-sliding-type TENGs										
Ball-Bearing-Type TENG	Steel balls, PTFE balls, and Aluminum	Semisolid Lubricant (Super Lube®)	100 rpm	-	40 V	6 mA	-	-	-	[86]
Ball-Bearing-Type TENG	Steel balls, PTFE balls, and Aluminum	Semisolid Lubricant (Super Lube®)	300 rpm	-	35 V	1 mA	35 mW @ 1 MΩ	80% 990,000 rotation	LEDs, capacitor charging	[86]
RF-TENG	Copper, PI, and ABS	Dry	60.15 N, 125 mm/s	-	432.7 V	0.55 μA	-	-	-	[92]
ORF-TENG	Copper, PI, and ABS	Hexadecane	60.15 N, 125 mm/s	-	1256.7 V	5.14 μA	1.14 mW	-	50 commercial LEDS lit	[92]

TENG = triboelectric nanogenerator, cTENG = case-encapsulated TENG, DLSS = dielectric liquid-based self-operating switch, LLS = liquid lubricant submerged, CL = composite lubricant sliding, NFCL = nano-film composite lubricated, TSS = triboelectric speed sensors, HS = hexadecane-containing sandwich structure based, TC = tribological behavior-controlled, PAO4 = Polyalphaolefin SpectraSyn 4, PFA = Perfluoroalkoxy alkane, ERB film = earthworm-inspired self-replenishing bionic film, it is a porous THV (TFE+HFP+VDF) terpolymer film modified with SiO_2 and saturated by squalane oil, CE = charge excitation strategy, GL = grease lubricated, TEIASS = triboelectric instantaneous angular speed sensor, SF = sliding freestanding, HSMs = hallow SiO_2 microspheres, TAB-TENG = a textured film and self-adapting contact synergized bidirectional rotary TENG, PAO = poly-alpha-olefin, ORF-TENG = an oil enhanced rolling friction based TENG, ABS = acrylonitrile butadiene styrene plastic.

3. Strain-Induced Electrification Nanogenerator (SIE-NG)

Recent research has mainly focused on addressing the challenges of friction and limited lifespan in TENGs, which stems from friction-induced wear, by employing solid, semisolid, and liquid lubricants as effective solutions [3]. Although lubricants provide significant advantages in TENGs, lubricants suffer drawbacks when employed, which in turn affect their practical applications [3]. The lifetime of TENGs can be extended under solid lubrication by mitigating wear at the contact interface; however, identifying suitable materials remains challenging due to factors such as dielectric properties and thermal stability. In addition, when the contact interface is nonconformal, performance losses may arise as a result of air breakdown [3]. Although liquid lubricants denote a promising approach, they can complicate the structural design of TENGs, making them less practical for biomedical and wearable applications, where simplicity and miniaturization are critical requirements [3]. Noncontact TENGs present an alternative approach, inherently eliminating friction and wear. However, their power generation capability is generally

limited, making them more appropriate for sensor applications rather than for fully self-powered systems [3].

Recently, Moon et al. [3] introduced a unique and novel frictionless nanogenerator, referred to as a strain-induced electrification-based nanogenerator (SIE-NG), to overcome challenges such as frictional wear, air breakdown, and complicated designs [3]. The SIE-NG consists of an ultrathin gold (Au) metal layer deposited on a dielectric PET substrate. Its operating principle relies on the charge-transfer mechanism typical of conventional TENGs, driven by the natural tendency of surface potentials to reach equilibrium between contacting materials [3]. This unique structure of the SIE-NG eliminates the sliding or repeated contact and separation process observed in conventional TENGs by utilizing strain-induced variation in the work function to generate electrical energy [3]. Owing to strain-induced electrification, the Au/PET SIE-NG achieved a current density of 4.8 mAm^{-2} and a power density of 15 mWm^{-2} at a low frequency of 0.5 Hz under a tensile strain of 0.21% and a load of 1.5 [3].

Figure 5 shows the strain-induced electrification (SIE) in an ultrathin Au metal layer deposited on PET, representing the electrification of the metal–dielectric interface. Notably, Au exhibits significant variation in work-function under mechanical strain, whereas insulator PET maintains a relatively stable work function under similar situations [3]. Contact electrification in conventional TENGs and strain-induced electrification in SIE-NGs are illustrated in Figures 5a and 5b, respectively. When the dielectric and metal come into contact, electron transfer occurs across the potential barrier during contact electrification [3,100]. Moreover, the surface roughness of materials creates unavoidable micro air gaps during contact, resulting in an additional barrier to charge transfer and thereby reducing the efficiency [3]. In contrast, SIE enables efficient electron transfer across the metal–insulator interface (Figure 5b) [3]. Under the application of external mechanical strain on the ultrathin SIE-NG structure, the equilibrium states of adjacent dielectric–metals became disordered, particularly when the metal material exhibited a change in work function while the work function of dielectric material remains stable [3,101]. Moreover, owing to the direct deposition of Au on the PET surface, no air gap existed, thereby enabling the smooth transfer of charges across the metal–insulator interface. Figure 5c and Figure 5d show the output current signal due to the contact electrification and strain-induced electrification, respectively.

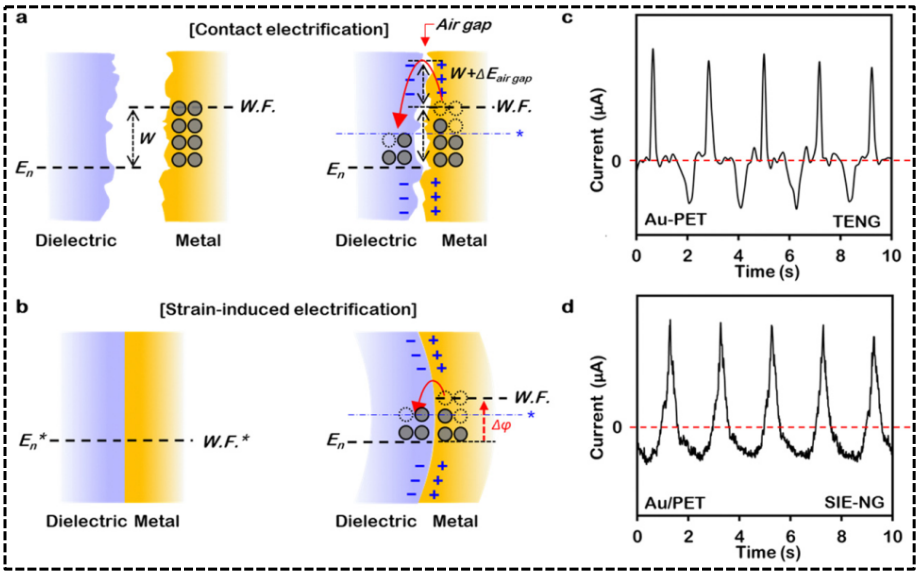


Figure 5. A surface-state diagram illustrating the electrification of the dielectric–metal interface, which indicates charge transfer between the dielectric and metal: (**a**) contact electrification when two materials

with differing electronegativities establish contact with each other; (**b**) strain-induced electrification while the surface potential is adjusted under a material-modified work function; this is considerably affected by mechanical strain, such as bending. (**c**) and (**d**) the instantaneous short-circuit current in (**c**) contact electrification and (**d**) strain-induced electrification. En, the neutral level of the surface state in the dielectric; * the energy level at the interface under equilibrium [3]. Reproduced from ref. [3], under CC. BY. 3.0 license.

4. Effect of Mass Fraction on Tribological and Triboelectrical Performance

The electrical and tribological performance of the CL-STENG, composed of copper–BTO/PI triboelectric layers under squalane, with varying mass concentrations of BTO nanoparticles (NPs) in PI film, was investigated by Li et al. [29]. It was observed that the Voc of the CL-STENG increased with an increasing BTO NPs concentration in the PI film up to 20 wt.%, after which it decreased. The maximum Voc was achieved at 20 wt.% of BTO NPs in the PI films. This increasing–decreasing trend in voltage was attributed to changes in the dielectric constant of the BTO/PI film with varying BTO NP concentrations [29]. The increased dielectric constant of the BTO/PI film created deeper charge traps, resulting in enhanced output. However, at higher concentrations, BTO NPs agglomerated within the PI film, leading to high dielectric loss, formation of leakage current paths in the composite film, and a decline in output [29].

The average COF of the CL-STENG decreased when the doping mass fraction of BTO NPs is below 20 wt.%, due to the rolling effect of nanoparticles. However, when the doping mass fraction exceeded 20 wt.%, the COF increases, which is attributed to the conglomeration of wear debris with BTO NPs at the friction interface [29]. This aggregation reduces the mobility of the nanoparticles, causing the plowing effect to dominate. A similar trend was observed for mass loss with varying doping mass fractions, with the optimal concentration of BTO NPs determined to be 20 wt.% [29].

The output current and friction coefficient of the steel ball–PVDF TENG are influenced by the volume of PAO oil lubricant. The current decreased gradually with increasing amounts of PAO lubricant. Initially, the current was 6 nA at a PAO quantity of 0.5 μL, but it decreased to 3 nA when the PAO quantity reached 5 μL [93]. Likewise, the COF decreased with increasing amounts of PAO oil lubricant. This indicates that a small quantity of PAO oil is sufficient to suppress air breakdown and enhance tribocharges at the contact interface, thereby increasing the current. However, although a larger amount of PAO can further inhibit air breakdown, it simultaneously reduces the effective contact area between the steel ball and PVDF [93].

The electrical output and friction coefficient obtained from the steel ball–PTFE TENG configuration under a load of 5 N, sliding speed of 200 mm/s, and varying graphene concentrations in silicone oil are presented in Figure 6a–c. The average COF values calculated within the 1800 s–2400 s (steady state) are shown in Figure 6c. In pure silicone oil, the COF is 0.027, whereas it decreases to 0.016 after the addition of 0.005 wt.% graphene nanosheets [88]. However, with further increase in graphene concentration, the average COF remains in the range of 0.024–0.029. Notably, the COF exhibits a sharp drop only at the low mass fraction of graphene (0.005 wt.%), reaching a steady-state value of 0.016 within a short time [88]. Figure 6a,b shows the Isc and Voc of the steel ball–PTFE TENG under silicon oil and graphene-doped silicone oil lubrication. In pure silicon oil lubrication, the steel ball sliding against the PTFE sheet generates a current of 1.64 nA and a voltage of 0.62 V. In contrast, it produces a maximum current of 2.42 nA and a voltage of 0.92 V at 0.1 wt.% graphene-doped silicon oil lubrication [88]. The friction coefficient, current, and voltage values are summarized in Figure 6c. It is observed that 0.005 wt.% graphene-doped silicon oil lubrication achieves the lowest COF of 0.016, with a corresponding current of 2.14 nA and voltage of 0.77 V [88].

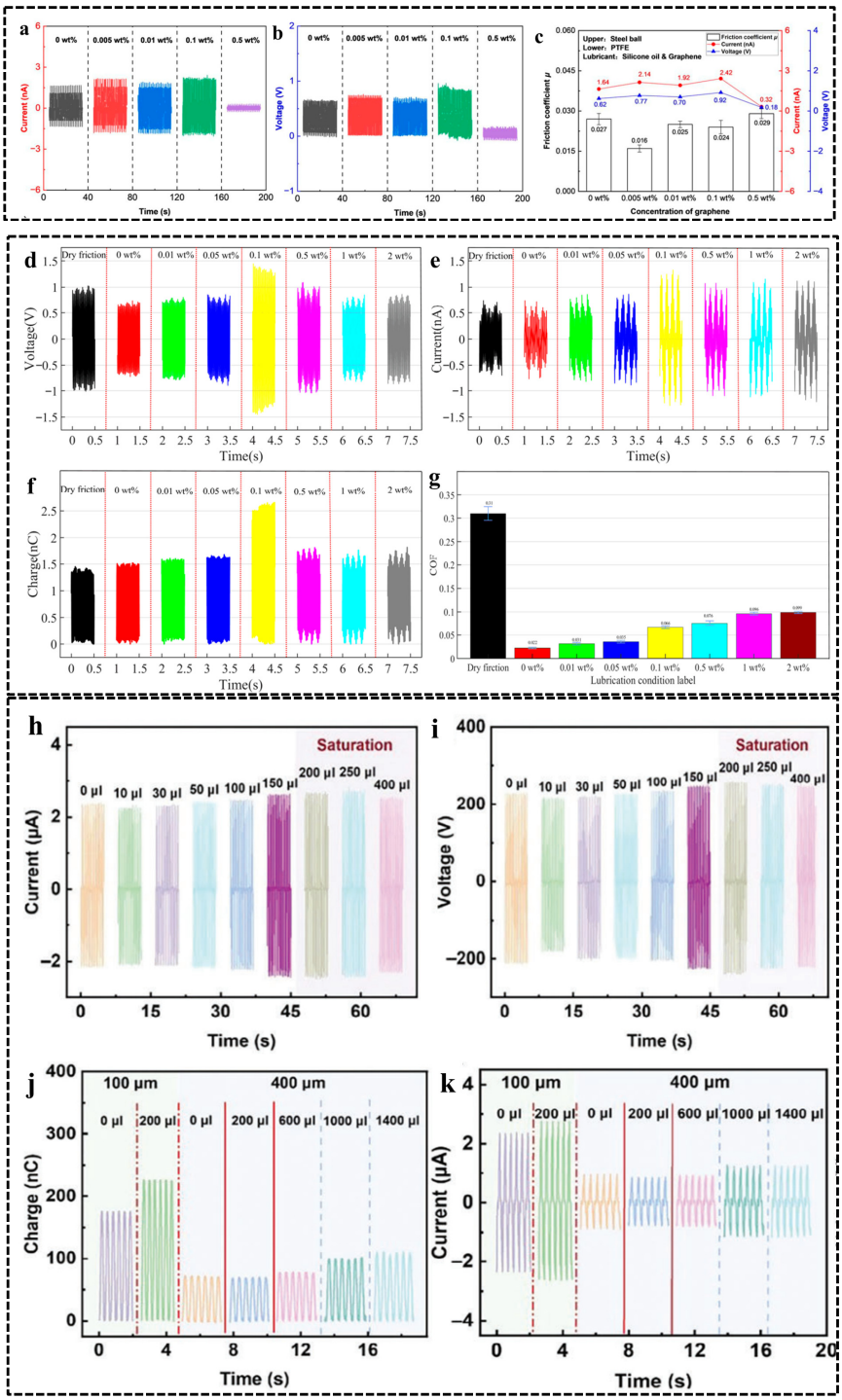


Figure 6. The electrical and friction performance of the steel ball–PTFE film under graphene-doped silicone oil lubrication (load—5 N, sliding speed—200 mm/s). (**a**) The short-circuit current, (**b**) the open-circuit voltage, and (**c**) the average friction coefficient, maximum short-circuit current, and maximum open-circuit voltage. Reproduced from ref. [88] under CC BY 4.0 license. Triboelectrical and tribological performances of the PI film–steel ball under TiO_2-doped oleic acid lubrication (load—5 N, velocity—80 mm/s). (**d**) The output open-circuit voltage, (**e**) the output short-circuit current, (**f**) the effective charge, and (**g**) the average COF. Reproduced from ref. [94] under CC By 4.0 license. The output performance of ERB-TENG. The effect of lubricant volumes on (**h**) short-circuit currents, and (**i**) output voltages of PT/SiO_2 films, comparisons of (**j**) transferred charge, and (**k**) short-circuit current, for 100 and 400 μm thick PT/SiO_2 films of changing squalane contents. Reproduced from ref. [98] under CC BY 4.0 license.

The friction and wear of the materials under sliding contact can be effectively reduced in the presence of liquid lubrication compared to dry conditions. The presence of lubricants forms a protective film that minimizes direct contact between the surfaces, thereby reducing friction [94]. The friction and triboelectrical performance of the PI film sliding against a steel ball under dry conditions and various TiO_2-doped oleic acid lubrications were investigated, and the results are presented in Figure 6d–g. Spherical nanoparticles can be effectively used as additives to improve the tribological properties; hence, TiO_2 nanoparticles were incorporated into oleic acid, with concentrations varied in the range of 0–2 wt.% [94]. The output Voc gradually increased with increasing TiO_2 concentration up to 0.1 wt.% and then decreased as the concentration continued to increase (Figure 6d). The maximum Voc of ~1.4 V was observed at 0.1 wt.% TiO_2 doping in oleic acid, which is higher than the Voc of ~1.0 V under dry conditions. In contrast, the output Voc under pure oleic acid was ~0.6 V, lower than that under dry conditions, indicating that oleic acid alone does not improve triboelectric performance [94]. Therefore, the triboelectric performance of oleic acid is improved by the addition of TiO_2 nanoparticles. Likewise, as shown in Figure 6e,f, the maximum current (~1.3 nA) and charge (~2.6 nC) values are observed at 0.1 wt.% TiO_2 doping in oleic acid. The improved performance of oleic acid lubricant arises from the doping of TiO_2 that helps the charge accumulation and electron flow in TENGs [94]. Overall, the voltage, current, and charge increase with increasing TiO_2 concentration, and 0.1 wt.% TiO_2-doped oleic acid showed the best triboelectrical performance.

Figure 6g shows the average COF of PI sliding against the steel ball under the dry and lubricated conditions. The average COF under the dry condition is 0.31. It sharply decreases to 0.022 in the presence of oleic acid, owing to its lubrication effect. However, the addition of TiO_2 (0.01 wt.%) into oleic acid increases the average COF. At 0.1 wt.% TiO_2, COF rises to 0.066, and it further increases to 0.099 at 2 wt.% TiO_2 doping. Thus, the COF increases with increasing TiO_2 concentration in oleic acid. This increased friction can be attributed to the non-homogeneous dispersion of TiO_2 particles, their accumulation on friction surfaces through interaction, and excessive presence of TiO_2 particles relative to oleic acid [94].

Guo et al. [97] investigated the influence of OLC mass fraction in hexadecane lubricant on the current and friction coefficient of a freestanding-mode TENG based on a steel–PTFE pair. The hexadecane–OLC lubricant was prepared by varying the mass concentration from 0.005 wt.% to 0.5 wt.% in hexadecane. The electrical current output and charge transfer of the TENG initially increased with rising OLC concentration up to 0.05 wt.%, after which both current and charge transfer decreased with further increasing OLC concentration. However, the friction coefficient showed different behavior than current and charge transfer; the friction coefficient decreased first and later increased with OLC concentration in hexadecane [97]. In addition, the wear volume of PTFE film was significantly reduced under hexadecane–OLC lubrication compared to the dry condition. It was concluded that an appropriate hexadecane–OLC lubricant concentration enhanced the electrical output performance, while reducing the wear and friction behavior of PTFE films [97].

Figure 6h,i show the current and voltage of the PT/SiO_2-Cu-based TENG under varying amounts of squalane. The PT/SiO_2-Cu TENG achieved its maximum electrical output at 150 μL squalene (Figure 6h,i). Beyond this, the electrical output showed a little variation, which may indicate that the PT/SO_2 film had reached its squalane saturation level [98].

The thickness of the PT/SiO_2 film is expected to strongly influence its oil absorption capacity, making it essential to examine whether thicker films require greater amounts of lubricating oil [98]. To investigate this, a PT/SiO_2 film with a thickness of 400 μm was fabricated and tested to evaluate the effect of lubricant content on output performance. As

shown in Figure 6j,k, the 400 μm film exhibited significantly lower output compared with the 100 μm film in the absence of lubricant, a result attributed to the weakened electrostatic induction at the bottom electrode with increasing thickness [98]. Interestingly, when 200 μL of lubricant, the same amount used for the 100 μm film, was added, the output of the 400 μm film showed little improvement, whereas the thinner film (100 μm) displayed a clear enhancement [98]. Only after increasing the lubricant volume to 1000 μL did the 400 μm film demonstrate a substantial and stable improvement in output performance (Figure 6j,k). These findings highlight a positive correlation between film thickness and oil storage capacity, indicating that thicker films demand larger volumes of lubricant to achieve effective lubrication, ideally approaching an oil absorption saturation state [98].

5. Effect of Load on Tribological and Triboelectrical Performance

The operation of TENGs significantly relies on the effective contact of triboelectric materials that constitute the device, which ultimately depends on the externally applied load. The load influences the friction state between the two contacted tribomaterials in TENGs, and hence, affects both their tribological and triboelectrical performance. The FS-TENG under both air and squalane lubrication conditions showed increasing open-circuit voltage, short-circuit current, and transferred charge with rising applied load. This is because, with increasing load, the triboelectric pair contact becomes more efficient, thereby improving the triboelectrification efficiency [62]. Further, the sliding FS-TENG showed higher electrical performance under liquid lubrication compared to air conditions, due to the suppression of air breakdown at the contact interface by the liquid lubrication [62].

The effect of the load on the current generated during the friction process between the steel ball and PVDF was investigated. As the load increased from 1 to 8 N, the current rose from 1 to 4 nA. With increasing load, the COF decreased, and the contact area between the two friction materials expanded, thereby improving the ratio of contact area to load, enhancing triboelectric charge generation, and increasing the current [93]. However, when the load exceeded 6 N, the change in current became negligible. The maximum effective contact area was achieved at 6 N, and further increases in load had only a limited effect on charge generation [93].

Figure 7a shows the friction coefficient curves of PTFE films sliding against a steel ball under a graphene-doped silicone oil lubrication, with applied loads ranging from 1 to 10 N. At 1 N, the COF curves exhibit greater fluctuations compared to higher loads, with values varying in the range of 0.017 to 0.025. The average COF at 1 N is 0.022, which gradually decreases to 0.012 as the load increases to 10 N [88]. Figure 7b shows the maximum Isc and Voc under different loads operating with graphene-doped silicon oil lubrication. Both the maximum Isc and Voc increase significantly as the load rises from 1 N to 10 N. Specifically, the maximum Isc increases from 1.52 nA to 3.13 nA, while the maximum Voc increases from 0.36 V to 0.99 V (Figure 7b) [88].

Wu et al. [30] evaluated the effect of external mechanical pressure on the Voc of a slide-mode TENG composed of PI film and Al film under dry friction and squalane lubrication. The open-circuit voltage was measured in a relatively stable state and is given in Figure 7c. Under dry sliding conditions, the voltage increased with the load up to 15 N, but the PI or Al films broke at 20 N, leading to a decrease in voltage. In contrast, the PI-Al shows continuously increasing and higher voltage under squalene compared to dry friction as the load increases from 5 N to 20 N [30].

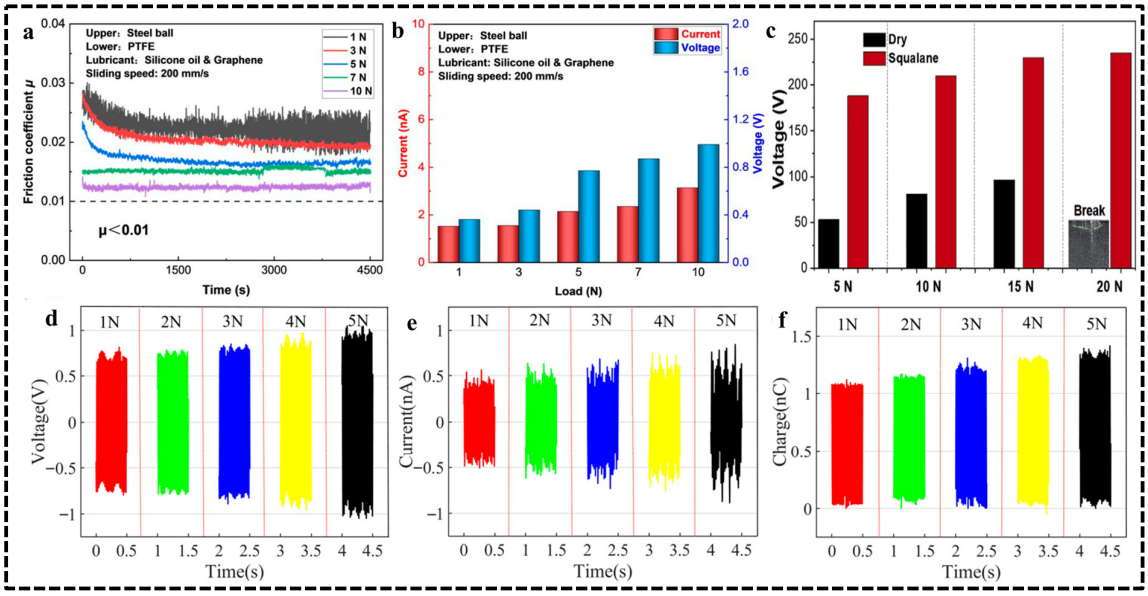


Figure 7. Triboelectrical and tribological performances of the PTFE film sliding against a steel ball under the graphene-doped silicone oil (0.005 wt.% graphene) lubrication condition with different loads (1 N to 10 N). (**a**) Friction curves with a sliding speed of 200 mm/s, and (**b**) the maximum short-circuit current and open-circuit voltage with a sliding speed of 200 mm/s. Reproduced from ref. [92] under CC BY 4.0 license. (**c**) The voltage of the PI-Al contact under dry friction and squalane lubrication conditions at varying applied loads. Reproduced from ref. [30], Copyright (2020), Elsevier. The electrical output of the steel ball–PI film contacts at varying loads (1 N to 5 N) under dry friction. (**d**) The open-circuit voltage, (**e**) short-circuit current, and (**f**) transferred charge. Reproduced from ref. [94] under CC BY 4.0 license.

Wang et al. [95] investigated the influence of applied load on the electrical output and friction coefficient of a liquid superlubric rotating TENG composed of a PTFE ball and an ITO-coated glass substrate. The Voc and Isc of the liquid superlubric TENG were 0.42 V and 43.2 nA, respectively, at an applied load of 3 N. When the applied load was increased to 17.5 N, the Voc and Isc rose to 1.03 V and 102.4 nA, respectively. Furthermore, at 17.5 N, these Voc and Isc values were 53.0% and 58.4% higher, respectively, compared with those of the lubricant-free TENG [95]. The COF of the lubricant-free TENG fluctuates only within a narrow range of 0.2598–0.2705 as the normal load increases from 3 N to 17.5 N, indicating significant wear. In contrast, the liquid superlubric TENG exhibits a decrease in friction coefficient from 0.0106 to 0.0047. Notably, the liquid superlubric TENG entered the superlubricity regime (COF < 0.01) within 10 s. At a normal load of 17.5 N, its COF is reduced by 98.2% compared with that of the lubricant-free TENG [95].

The effect of the applied load on the triboelectrical properties was investigated by Shao et al. [94]. The voltage, current, and charge generated during the sliding of PI film against a steel ball under dry conditions with varying loads from 1 N to 5 N are illustrated in Figure 7d–f. The triboelectric output is lower at an applied load of 1 N, and it is higher at 5 N, indicating the significant influence of applied load on voltage, current, and charge generation during the sliding process of PI films against a steel ball under dry conditions (Figure 7d–f) [94].

The effect of the applied load on the friction and electrical output of freestanding TENGs was explored under dry, hexadecane, and hexadecane–OLC lubrication conditions. Under dry friction, TENGs showed increased current and voltage with increasing applied normal load, owing to the increased contact area between the PTFE and steel sheets, whereas their COF initially increased and later decreased with the load [97]. After the addition of hexadecane and hexadecane–OLC, the TENGs showed an increasing trend of

electrical output with the load only in the case of hexadecane–OLC. Both hexadecane and hexadecane–OLC did not show much variation in COF with increasing load and remained relatively stable [97].

The variation in output voltage and current produced from the PT/SiO_2 film and ERB film sliding against the copper under different loads ranging from 1 N to 20 N was discussed by Liu et al. [98]. The electrical output initially rose with increasing load, plateaued at 5 N, and then remained stable with further increases. For the ERB-TENG, the electrical output rose with increasing load up to 5 N but subsequently declined, in contrast to the PT/SiO_2 with no lubricant. This decline can be ascribed to the excessive release of lubricant under high pressure, which reduces the effective interface area between the friction materials. These results suggest that regulating the liquid lubricant by controlling the external load is important for optimized performance of ERB-TENG [98].

6. Effect of Frequency on Tribological and Triboelectrical Performance

The influence of sliding velocity on the electrical output in cTENGs was investigated by Jing et al. [81]. A linear motor was used to apply reciprocating motion with velocities ranging from 0.3 to 1.0 m/s at a stroke length of 35 mm [81]. The electrical output is shown in Figure 8a,b. The short-circuit current of cTENGs increased with velocity and reached a maximum value of 668 μA at 1.0 m/s (Figure 8a) [81]. Moreover, the current increased linearly with sliding velocities. This behavior is expected because higher velocity shortens the duration of a single charge–transport process, while the amount of transferable induced charges between electrodes remains constant. At the same time, the frequency of the output current is also linearly enhanced [81]. In contrast, sliding velocity does not significantly influence the Voc of cTENG, which fluctuates within the range of 110–130 V (Figure 8b) [81].

The NFCL-TSS exhibited an almost constant Voc and short-circuit charge across motor speeds ranging from 10 to 3000 rpm. However, with increasing motor speed from 10 to 3000 rpm, the Isc increased from nearly 0 μA to 11 μA. The output voltage is high and more stable, making it suitable as an input for signal processing circuits effectively [29].

The output triboelectric signal of the steel ball–PVDF friction pair lubricated with 0.5 μL PAO was evaluated at various frequencies. The Isc increased with frequency and reached 8 nA at 4 Hz [93]. As the frequency of motion rose, the friction between the two materials intensified, leading to a larger effective contact area and, consequently, a higher output current [93]. Figure 8c shows the COF curves of PTFE films sliding against a steel ball under a graphene-doped silicone oil lubrication, with sliding speeds ranging from 200 mm/s to 1000 mm/s. It is seen that the average COF gradually decreases from 0.012 to 0.008 as the sliding speed increases from 200 mm/s to 1000 mm/s. Notably, at a sliding speed of 1000 mm/s, with an applied load of 10 N, the COF of the PTFE film sliding against a steel ball drops below 0.01 under graphene-doped silicone oil, indicating the achievement of a superlubric friction state [88]. Figure 8d presents the maximum Isc and Voc generated during the sliding of the PTFE film against the steel ball. As the sliding speed increased from 200 mm/s to 1000 mm/s, the maximum Isc rose markedly from 3.13 nA to 8.49 nA. In contrast, the maximum Voc reached a steady state, fluctuating within the range of 0.91–0.99 V [88].

The electrical output performance of rotary sliding FS-TENG in air and liquid lubrication at frequencies ranging from 1.0 Hz to 3.0 Hz is shown in Figure 8e,f. Compared to TENGs operating in air, the interface liquid-lubricated TENGs show enhanced transferred charge and Isc performance at all tested frequencies. Moreover, the current increases with increasing frequency. The maximum current and transferred charge achieved by the liquid-lubricated TENGs were 150 μA and 5 μC at 3.0 Hz, respectively [62].

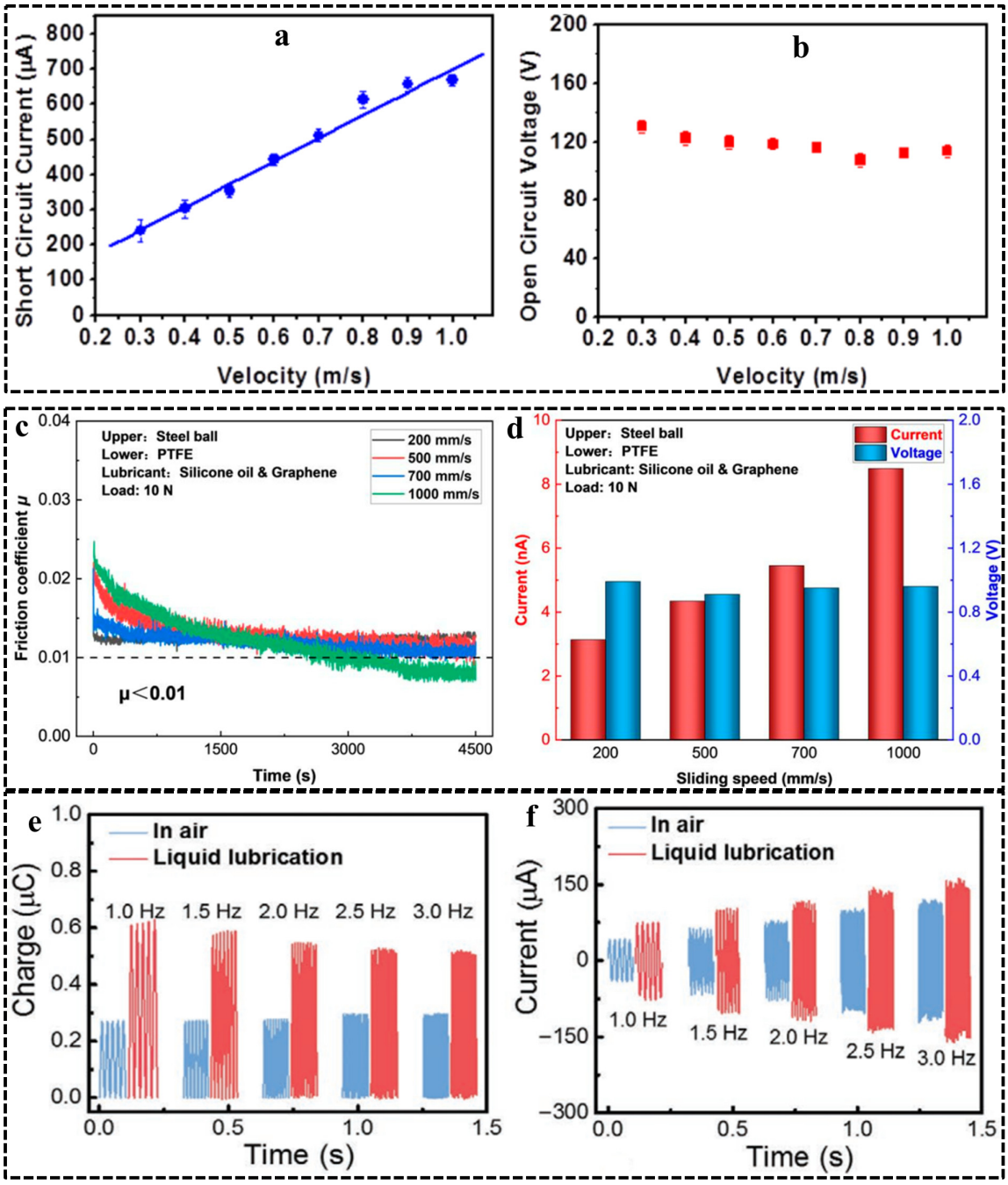


Figure 8. The output current and voltage characteristics of cTENG. (**a**) Current peak values, and (**b**) voltage peak values over various sliding velocities. Reprinted with permission from ref. [81], Copyright (2014), American Chemical Society. The friction coefficient, current, and voltage output of the PTFE film sliding against a steel ball under the graphene-doped silicone oil (0.005 wt.% graphene) lubrication condition with various sliding velocities (200 mm/s to 1000 mm/s). (**c**) Friction curves at a load of 10 N with various sliding velocities, and (**d**) the maximum short-circuit current and open-circuit voltage under various sliding velocities with a load of 10 N. Reproduced from ref. [88] under CC BY 4.0 license. (**e**) The transferred charge and (**f**) short-circuit current of rotary sliding FS-TENG under air and interface liquid lubrication. Reprinted with permission from ref. [62], Copyright (2020), Wiley.

Guo et al. [97] observed an increase in the current, voltage, and charge output of a freestanding TENG composed of PTFE and a steel sheet with gradually increasing frequency from 0.5 Hz to 4 Hz, under dry, hexadecane, and hexadecane–OLC lubrication conditions. This behavior is attributed to the higher rate of mechanical energy input with increasing

frequency, which enhances the interfacial triboelectric efficiency [97]. The COF of the TENG under dry conditions increased with sliding frequency, whereas it was reduced under hexadecane and hexadecane–OLC lubrication. In the case of dry friction, the rise in COF with frequency can be attributed to the formation of microscopic "furrows" in the real contact area as the two surfaces repeatedly slide against each other [97]. With higher frequency, more furrows are generated, producing additional PTFE wear debris. While a small portion of this debris is expelled from the contact track, most particles remain trapped and are continuously transferred and adhered through the reciprocating motion of the friction pair. This accumulation enhances interfacial adhesion and meshing between surface asperities, thereby elevating the COF [97]. In contrast, under hexadecane and hexadecane–OLC lubrication, the COF gradually decreased with increasing frequency. This reduction occurs because the wear debris generated at higher frequencies is more readily removed from the contact zone by the flowing lubricant, which diminishes interfacial adhesion and asperity interlocking, resulting in a lower COF [97].

The liquid superlubric TENG lubricated with hexadecane demonstrates excellent performance. Owing to the presence of hexadecane, the Voc and Isc are enhanced by 52.7% and 48.9%, respectively, compared with the lubricant-free TENG, reaching 0.59 V and 61.7 nA. At the same time, the friction coefficient decreases by 98.4%, reaching as low as 0.0042 [95]. The effect of rotation speed on the electrical performance of the hexadecane-lubricated liquid superlubric TENG was further examined. As the rotation speed increased from 50 rpm to 400 rpm, the Voc rose from 0.09 V to 0.84 V (an 833.3% increase), while the Isc increased by 942.2%, reaching 86.5 nA. Both parameters improved at a much faster rate than those of the lubricant-free TENG [95].

The influence of rotation speed on the COF of hexadecane-lubricated TENG was also investigated. With increasing speed from 50 rpm to 400 rpm, the friction coefficient of the hexadecane-lubricated TENG gradually decreased from 0.0066 to 0.0031, corresponding to a 53.0% reduction [95]. In contrast, the COF of the lubricant-free TENG exhibited an upward trend with rotation speed. At 400 rpm, its COF reached 0.2614, which is 84.3 times higher than that of the liquid superlubric TENG. These findings confirm that the superlubricity state induced by lubricating oils (PAO and hexadecane) significantly reduces friction in the liquid superlubric TENG [95]. The instantaneous energy conversion efficiency was estimated as the ratio of electrical output power to frictional input power [95]. The results show that the liquid superlubric TENG achieves a far higher efficiency than the lubricant-free TENG. For instance, under a normal load of 17.5 N, a rotation speed of 300 rpm, and a rotation radius of 10 mm, the maximum Voc and Isc increased by 53.0% and 58.4%, respectively, while the COF decreased by 98.2% [95]. Consequently, the instantaneous energy conversion efficiency of the liquid superlubric TENG was 134.64 times greater than that of the lubricant-free TENG, underscoring its extraordinary advantage [95]. The influence of varying sliding velocities of PI films against a steel ball under dry conditions on the generated voltage, current, and charge is shown in Figure 9a,b,c. It clearly shows that the triboelectrical performance, voltage, current, and charge are higher at higher sliding velocities [94].

The electrical performance of the Au/PET-based SIE-NG device under varying motion frequencies is shown in Figure 9d–f. The voltage, current density, and power density increased as the frequency rose from 0.01 Hz to 0.5 Hz (Figure 9d–f). At 0.01 Hz, the SIE-NG generated a voltage of 1.61 V, a current density of 2.3 $mAm^{-2,}$ and a power density of 3.71 mWm^{-2}. These results show that the SIE-NG can effectively convert ultralow-frequency mechanical energy into electricity, unlike conventional TENGs, which often fail under such situations [3].

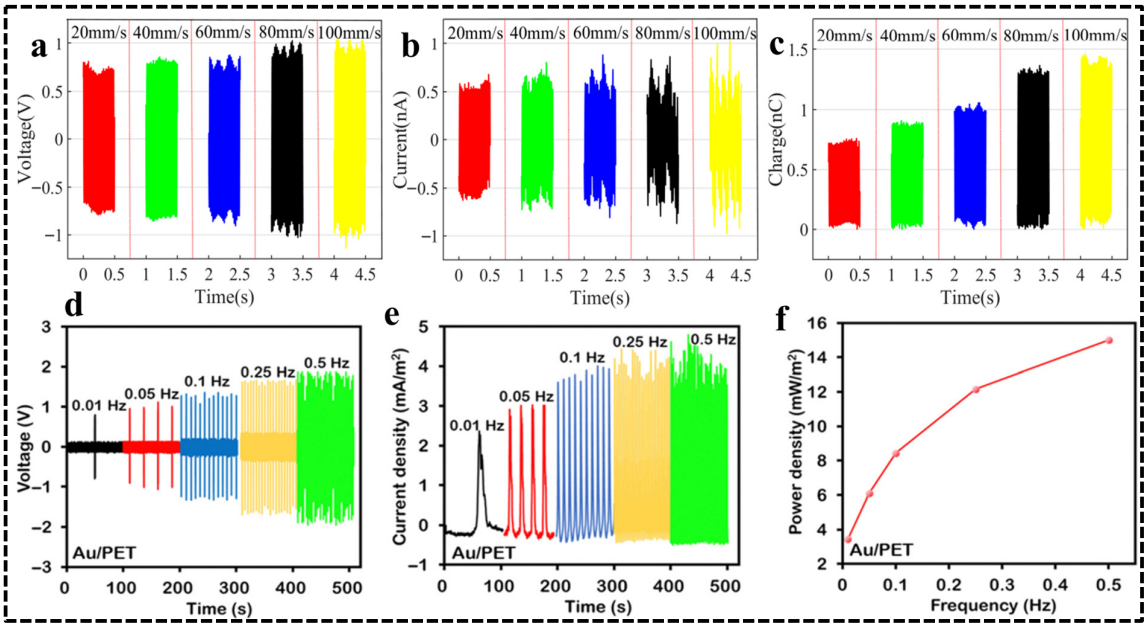


Figure 9. The triboelectrical output of the PI film–steel ball with changing velocities (20 mm/s–100 mm/s) under dry conditions. (**a**) The open-circuit voltage, (**b**) short-circuit current, and (**c**) transferred charge. Reproduced from ref. [94] under CC BY 4.0 license. The triboelectrical output of SIE-NG based on the Au/PET, with a tensile strain of 0.21%: (**d**) output voltage, (**e**) current density, and (**f**) power density, with frequencies ranging from 0.01 Hz to 0.5 Hz at an applied load of 1.5 Ω. Reproduced from ref. [3] under CC. BY. 3.0 license.

7. The Durability of the TENGs

The mechanical durability, in terms of the electrical output of the TENG devices, is an imperative parameter for exploring their potential applications. Sliding-mode TENGs suffer significantly from abrasion and wear of the triboelectric materials, especially under dry friction, which hampers their lifetime and durability. During sliding, excessive external force increases surface friction, thereby reducing energy conversion efficiency and compromising mechanical durability. Therefore, this section discusses the stability of various TENG devices operating under lubrication conditions.

The stability of the LLS-TENG device was evaluated over 72 h (432,000 cycles) by measuring the Voc. The result shows remarkable stability of the LLS-TENG by maintaining the constant Voc output throughout the 72 h test [83]. The liquid lubricant enhances TENG performance by increasing electrical output, extending mechanical lifespan, and reducing wear through rolling friction. With rolling electrodes and lubrication, the device achieves higher current output and minimizes friction damage [83]. The OA-TENG based on OA-PS (4.8%) and nylon-11 exhibited an excellent mechanical stability, maintaining its output current over more than 60,000 cycles [82]. A rotating wheel disk TENG composed of a PTFE-steel triboelectric layer with hexadecane–OLC lubrication showed long-term stability over 6 h, maintaining a stable current output [97]. The average peak voltage of the ball-bearing TENG decreased from an initial value of 65 to 50 V after continuous operation for 55 h (990,000 rotations) at 300 rpm. This decrease to only 80% of the initial value suggests the remarkable stability of the ball-bearing TENG [86].

Figure 10a shows the long-term stability of the sliding FS-TENG, evaluated under air and squalane liquid lubrication conditions over 500,000 operating cycles. The lubricated sliding FS-TENG displays outstanding electrical stability, maintaining 86% of its output with 152 nC, whereas the device operated in air retains only 9% of its electric output with a low initial value of 70 nC [62]. The electric stability of the rotary sliding FS-TENG, with

and without liquid lubrication, was evaluated over 100,000 working cycles by measuring the transferred charge, as shown in Figure 10b. The normal TENG shows a sharp decline in transferred charges, decreasing by 35% within only 12,000 cycles. In contrast, the rotary sliding TENG with interface liquid lubrication shows stable transferred charge output over 100,000 operating cycles, exhibiting remarkable durability, with only a 10% decline in electric output was observed [62]. In addition, the surface of the Kapton film in normal operation has several scratches (Figure 10c), whereas under lubrication, it shows only slight scratches (Figure 10d), suggesting the improved stability of the TENG and highlighting the advantage of liquid lubrication in all types of sliding TENGs [62].

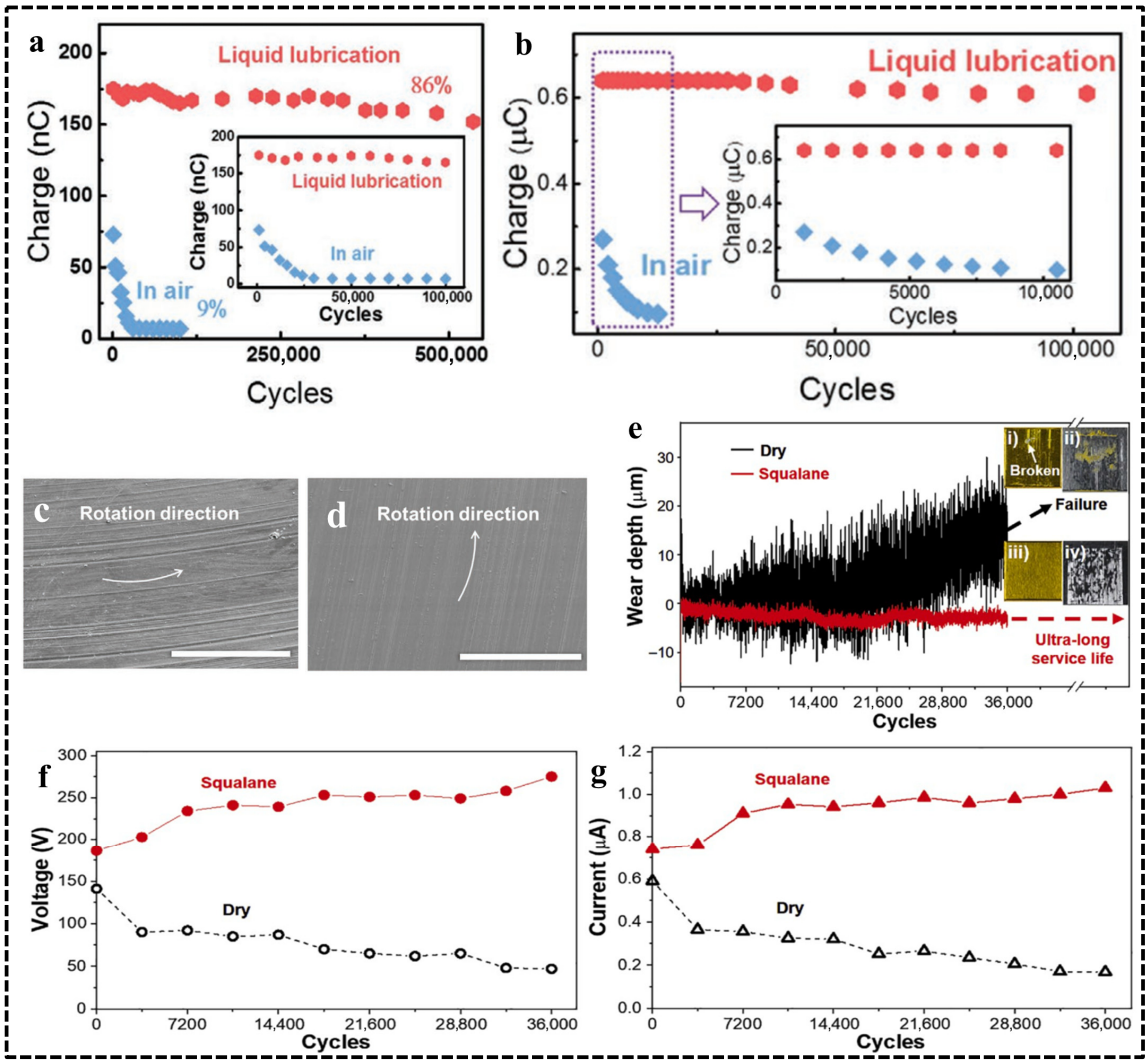


Figure 10. The stability of (**a**) the sliding FS-TENG, and (**b**) the rotary sliding FS-TENG under air and liquid lubrication conditions. Kapton film SEM images after 100,000 cycles in (**c**) air and with (**d**) interface liquid lubrication (scale bar, 300 mm). Reprinted with permission from ref. [62], Copyright (2020), Wiley. The long durability of the wear and electric outputs of PI-Al contacts under dry and squalane-lubrication conditions. (**e**) The wear depth and photos (inset) of the worn surfaces, (**f**) voltage, and (**g**) current at various cycles. Reproduced from ref. [30], Copyright (2020), Elsevier.

Figure 10e shows the wear depth of the PI-Al contact under dry and squalane lubrication conditions over several cycles, while the corresponding voltage and current are shown in Figures 10f and 10g, respectively. The results show a continuous increase in wear depth with increasing cycles, whereas both voltage and current decreased under solid–solid contact of PI-Al [30]. The polymer PI film has a very low thickness, which cannot sustain wear

under dry friction during operation, ultimately resulting in the failure of the TENG at a later stage [30]. As shown in Figure 10e, the durability of the PI-Al lubricated with squalane is remarkably improved, as evidenced by the stable wear depth even after 36,000 cycles. It is seen that when the contact is well lubricated, the wear remains very low [30]. Under liquid lubrication, the voltage and current of the PI-Al TENG initially increase continuously with the number of cycles and later stabilize, remaining higher compared to those of the TENG under dry friction [30].

The sliding-mode LP-TENG operating under silicon oil retains 90% stability over 500 k cycles, whereas the sliding-mode LP-TENG in air exhibits only 40% retention over 40 k cycles [13]. Wang et al. [90] explored the influence of hexadecane on the durability of TENG by continuously generating electricity over an extended period. In the traditional TENG (without hexadecane), the output voltage rose rapidly from 3.6 V to 19.8 V within the first 850 s, then increased more gradually to a peak of 23.2 V at 2600 s. Beyond this point, the voltage steadily declined, dropping to 11.3 V after 6000 s, a 51% reduction from the maximum, indicating a limited durability of less than 6000 s [90]. In contrast, the HS-TENG exhibited exceptional durability and output performance. Its voltage quickly increased from 13.4 V to 55.4 V during the initial 5000 s, then continued to rise gradually, reaching a maximum of 83.0 V at 54,000 s. Remarkably, the voltage remained stable with no significant decrease over the following 10,000 s. Overall, the service lifetime of HS-TENG was more than ten times longer than that of the traditional TENG, clearly demonstrating that the hexadecane-containing sandwich structure greatly enhances both durability and electrical performance [90].

Shao et al. [94] verified the long-term stability of the 0.1 wt.% TiO_2-doped oleic acid lubricated TENG during continuous operation over 3600 s, and it was seen that the output voltage, current, and charges remained almost constant after prolonged sliding.

TENGs represent a promising approach for harvesting distributed, low-quality energy sources but are hindered by long-term abrasion and limited durability [98]. To overcome these challenges, an earthworm-inspired self-replenishing bionic film (ERB) was employed as the tribo-material in sliding-freestanding TENGs (SF-TENGs). The ERB features an interconnected 3D porous network capable of storing and releasing lubricant under cyclic mechanical stimuli [98]. The ERB film is a squalane oil-saturated porous THV polymer (PT) film modified with SiO_2 nanoparticles. The long-term durability is a crucial parameter for TENGs, ensuring reliable operation over an extended time [98]. Figure 11a,b display the remarkable durability of the ERB-TENG; its output voltage remained stable even after 35 days and reduced by only 1% after 100,000 operating cycles, indicating outstanding durability. In contrast, dense THV (DT)-based interfacial-lubricating SF-TENG (DL-TENG) with 200 μL squalane showed poor stability, with its output voltage dropping sharply by 77% after 100,000 cycles, highlighting the superior stability of the ERB-TENG [98].

Figure 11c illustrates the outstanding durability of the TAB-TENG device. The output voltage remains virtually unchanged, even after continuous operation for 350,000 cycles, highlighting that its remarkable stability is due to the combined influence of the soft flat rotator's self-adapting capability and the surface-textured PDMS/HSMs film's self-lubricating nature [99]. This performance emphasizes numerous key advantages: efficient bidirectional energy harvesting, enhanced contact intimacy, reduced rotary resistance, minimized wear, and improved electrical output. Together, these features position the TAB-TENG as a highly promising solution for practical biomechanical energy harvesting applications [99].

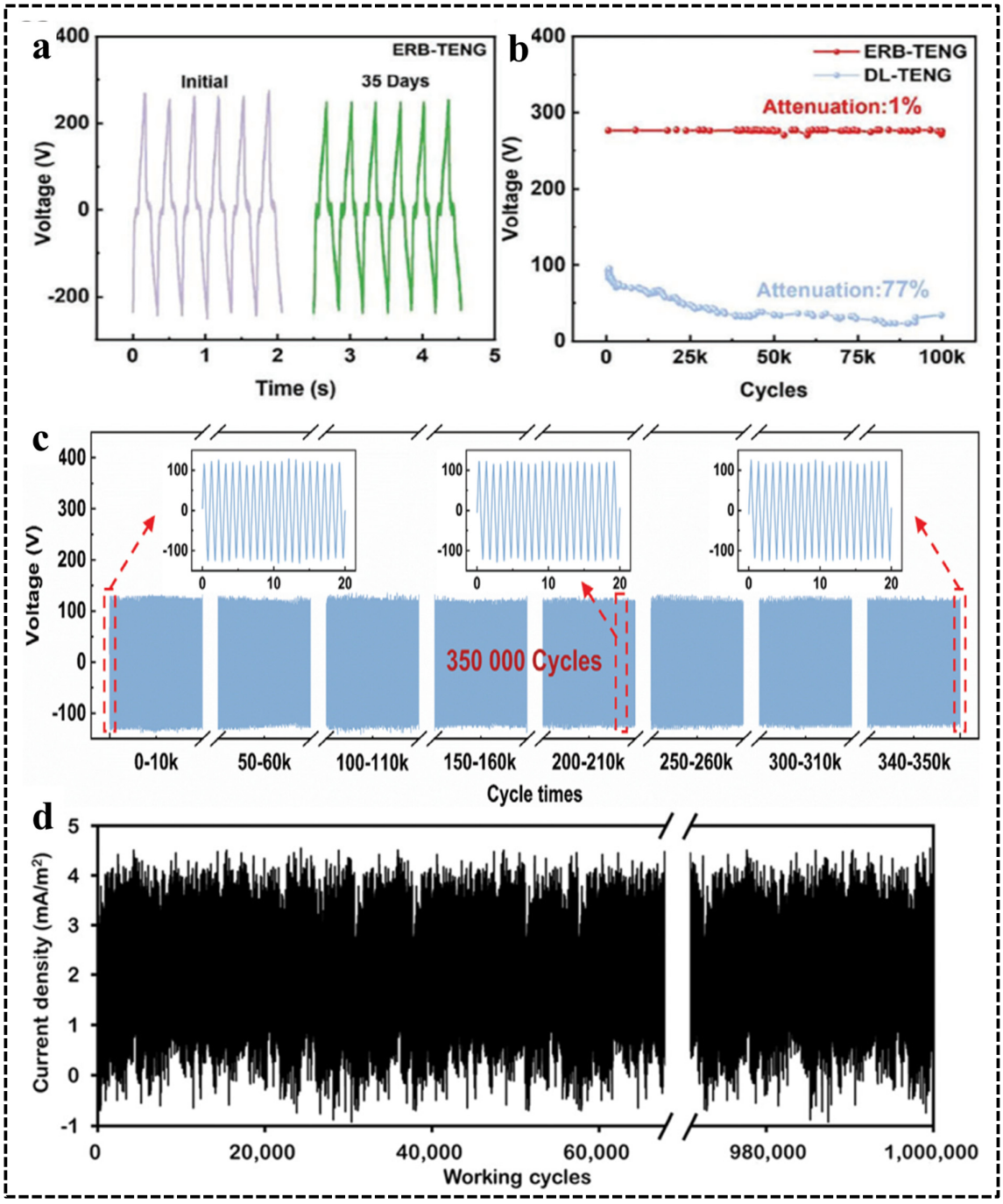


Figure 11. (**a**) The superior long-term output durability of the ERB-TENG over 35 days. (**b**) A comparison of the output voltage stability between the DL-TENG with 200 μL lubricant and ERB-TENG under continuous sliding friction for 100,000 cycles. Reproduced from ref. [98] under CC BY 4.0 license. The superior durability of the TAB-TENG. (**c**) The stability of the output voltage under continuous measurement for 350,000 cycles. Inset: magnified views of the first few peaks, the few peaks in the middle, and the last few peaks. Reprinted with permission from ref. [99], Copyright (2023), Wiley. The performance of the Au/PET-based SIE-NG with a tensile strain of 0.21%: (**d**) changes in the current density during cyclic bending for up to 1,000,000 cycles at a frequency of 0.25 Hz, with a tensile strain of 0.21%. Reproduced from ref. [3] under CC. BY. 3.0 license.

The long lifespan of the Au/PET-based SIE-NG was evaluated, as shown in Figure 11d. The device maintained a stable current density output without degradation over 1,000,000 working cycles, tested by bending under gentle human motions, thereby indicating its extraordinary stability. Due to the unique structural design, friction at the

interface is eliminated, allowing charges to be transferred smoothly and enabling the prolonged operation. These findings highlight the robustness of the device, addressing key challenges faced by conventional TENGs and showcasing its capability to scavenge ultralow-frequency mechanical energy [3].

8. Lubricant Properties and TENG Performance

In this section, the effect of lubricant properties, such as dielectric constant, conductivity, viscosity, permittivity, and polarity, on TENG performance is discussed.

8.1. Dielectric Constant and Conductivity

The dielectric constant of materials determines the electrical output performance of TENGs. The electrical output of TENGs arises primarily from triboelectric charge density and the subsequent electrostatic induction. Both triboelectric charge density and electrostatic induction are influenced by even slight changes in the dielectric constant of the materials. Charge accumulation is high in materials with a high dielectric constant, which leads to an enhancement in the TENGs' electrical output [67]. The dielectric properties of the triboelectric materials can be enhanced by forming a composite or by doping with high-dielectric materials, which eventually improves the electrical performance of TENGs by increasing the surface charge density [41]. The dielectric constant and charge retention capability of the pristine PDMS were altered by the addition of HSMS, resulting in a tenfold improvement in TENG performance compared to that of TENGs based solely on PDMS [99]. The electrical conductivity of the lubricant hampers the electrical output of TENGs, thereby highlighting its importance in TENG studies. Accordingly, the voltage of sliding-mode TENGs operating under different liquid lubricants, including squalane, castor oil, and CD15W-40, was examined. The electrical conductivity of squalane, castor oil, and Cd15W-40 was 2.1×10^{-8}, $1.2 \times 10^{-6,}$ and 0.15 µS/cm, respectively [29]. The results show that the steady-state output voltage of TENGs was significantly increased under squalane, while it decreased under the castor oil and CD15W-40 [29]. Both castor oil and CD1W-40, having higher conductivity than squalane, generated a negligible voltage output due to the neutralization of triboelectric charges. In contrast, squalane, with its low electrical conductivity, allowed triboelectric charges to remain largely unneutralized, resulting in the increased output voltage [29].

8.2. Viscosity and Polarity

The electric output performance of TENGs based on lubricants, particularly liquid lubricants, is affected by the viscosity of the lubricants, because the formation of the liquid film at the contact interface is largely influenced by the viscosity of the liquid [52]. Wu et al. [30] examined the influence of the dynamic viscosity of liquid lubricants on the output voltage of TENGs. The output voltage of the TENGs was obtained using several lubricants with varying viscosities, including heptane (0.388 mPa·s), squalane (31.123 mPa·s), paraffin oil (43.47 mPa·s), and PAO10 (132 mPa·s). Among these, the TENGs operating with heptane, which has the lowest dynamic viscosity, produced the highest output voltage, whereas PAO10, with the maximum viscosity, yielded the lowest output voltage [30]. Furthermore, it was reported that the low-viscosity liquids effectively increased the contact interface area of TENG materials by preventing the formation of transfer films and reducing air contact with TENG materials, ultimately enhancing the electrical output [30]. In another study, Chen et al. [88] observed that the maximum voltage and current for TENGs were obtained under squalane (28.94 mPa·s) compared with PAO6 (46.80 mPa·s) [88]. The TENGs operated with PAO (3.8 mPa·s) lubricant achieved 155.6% and 140.5% enhancement in the Voc and Isc, respectively, compared with the non-lubricated

TENG. In addition, the TENG reached the superlubric state with an initial friction coefficient of 0.0088 and eventually decreased to 0.0025 [95]. Polar and nonpolar liquids have shown a significant impact on the current and voltage output of TENGs. Polar liquids, such as PEG 200, water, Pluriol A 500 PE, and ionic liquid [Emim][NTf_2], exhibited very poor electrical performance of TENGs with negligible current and voltage. In contrast, paraffin oil, PAO10, and squalane, which are nonpolar liquids, demonstrated excellent electrical performance of TENGs with higher voltage and current output [30,52,90].

8.3. Permittivity

Along with viscosity, relative permittivity is also an important factor that determines the electric performance of TENGs. The electrical performance of TENGs based on liquid lubricant is influenced by the permittivity of the lubricant. It has been observed that liquids with low permittivity improve the electrical output of TENGs, whereas high permittivity leads to a reduction in performance [52]. Wu et al. [30] investigated the impact of the permittivity of lubricants on the electrical output of TENGs operating under various liquids. The output voltage of the TENGs was measured using heptane, squalane, paraffin oil, PAO10, olive oil, rapeseed oil, Pluriol A 500 PE, [Emim][NTf_2], PEG 200, and water. The relative permittivity of these liquids ranged from 1.92 to 80.1, with heptane showing the lowest values (1.92) and water exhibiting the highest (80.1) [30]. The voltage of the TENGs with low-permittivity liquids (heptane, squalane, paraffin oil, and PAO10) was higher compared to those with high-permittivity liquids (Pluriol A500 PE, PEG 200, and water). Due to the higher relative permittivity, the induced charges on the TENG materials could be neutralized, resulting in a lower output voltage. In contrast, the low-permittivity liquids restrict charge transfer, thereby generating a higher voltage output [30,90]. In another study, Zhao et al. [87] examined the open-circuit voltage of rotating TENGs using insulating grease, PTFE grease, fluorosilicone grease, and lithium grease with relative permittivity of 3.10, 3.35, 9.12, and 9.59, respectively [87]. Among these semisolid grease lubricants, insulating and PTFE greases showed enhanced Voc, whereas the Voc decreased under fluorosilicone and lithium greases. The enhanced Voc of TENGs with insulating and PTFE greases is attributed to their lower relative permittivity and dielectric loss [87].

9. Working Mechanism of TENGs in Air and Liquid Lubrication

Figure 12a illustrates the working mechanism of the LLS-TENG, which involves three key steps. First, negative charges on the PTFE surface layer induce positive charges in the rolling electrode. These charges are separated by the PTFE surface, with the negative charges accumulating on the opposite side. As the rolling electrode approaches the plate electrode, direct electron transfer occurs upon contact, amplifying the electrical output. The presence of liquid lubricant further enhances the surface charge of PTFE by suppressing air breakdown and extends the device's mechanical lifespan [83].

Figure 12b–d present the wear and output performance mechanism of TENGs under dry friction, oleic acid lubrication, and TiO_2-doped oleic acid lubrication conditions. The triboelectric charges are generated under the dry friction, which subsequently produces voltage and current. However, as shown in Figure 12b, the PI films experience severe wear, and some wear debris are transferred on the steel surface under intense dry friction. In addition, fragments of the worn PI films are scattered and re-adhered, which prevents further generation of triboelectric charges [94]. The oleic acid lubrication conditions reduce the severe wear and debris of the PI film, as shown in Figure 12c. The principal wear mechanism shifts to fatigue wear, marked by the formation of cracks slowly and the removal of material steadily from the PI interface. Also, the triboelectric performance shows only slight variation compared with that under dry friction conditions [94].

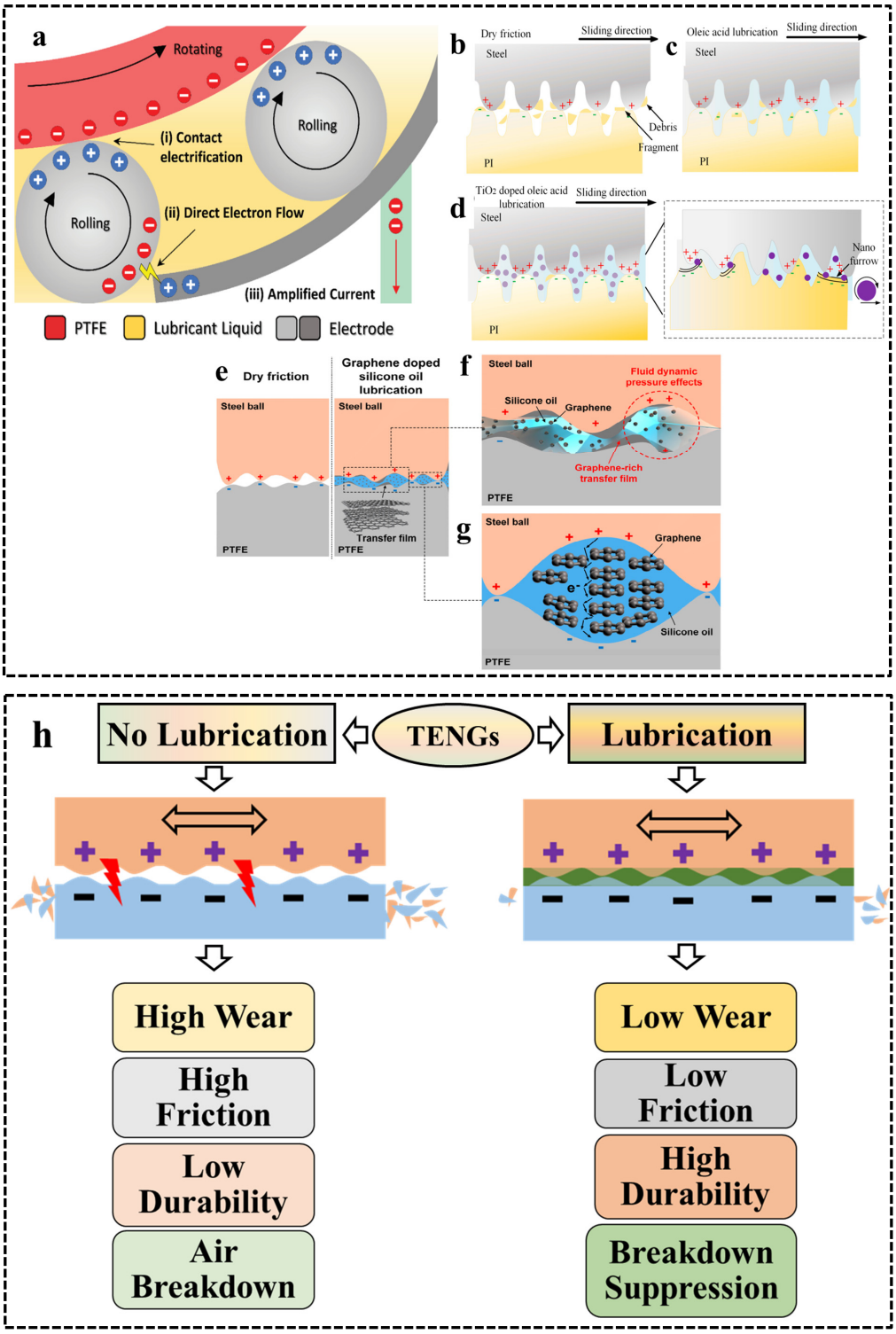


Figure 12. (**a**) A schematic of the working mechanism of the LLS-TENG. Reprinted with permission from ref. [83], Copyright (2021), Wiley. The mechanism of wear and output performances under various conditions. (**b**) Dry friction. (**c**) Under oleic acid lubrication. (**d**) Under TiO_2-doped oleic acid lubrication. Reproduced from ref. [94] under CC BY 4.0 license. The super-low friction electrification mechanisms for the PTFE film sliding against a steel ball under the graphene-doped silicone oil lubrication condition. € A macro-scale model for the PTFE film running against a steel ball under dry friction and graphene-doped silicone oil lubrication. (**f**) The super-low friction mechanisms. (**g**) The electron generation mechanisms. Reproduced from ref. [88] under CC BY 4.0 license. (**h**) An overview of TENG performance in non-lubricant and lubricant media.

The lubricant oleic acid with TiO_2 content significantly reduces the wear and debris formation of the PTFE film, as shown in Figure 12d. TiO_2 plays a crucial role in minimizing debris formation and simultaneously enhancing voltage and current output by promoting the generation of tribocharges [94]. Furrows on the surface of PI films occurred due to the sliding of TiO_2 nanoparticles across the film surface, a phenomenon known as the micro-machining effect [94]. This process increases the effective contact area and thereby improves triboelectrical performance. Thus, the oleic acid and TiO_2 together help wear reduction and electrical performance enhancement of PI films sliding against a steel ball. Moreover, the polar and nonpolar properties of oleic acid influence frictional charge generation and triboelectric performance upon contact with solid material, while also serving as a superior lubricant that reduces wear at the interface [94].

The super-low friction electrification mechanisms for the PTFE film sliding against a steel ball under the graphene-doped silicone oil lubrication condition are proposed, and schematic illustrations are shown in Figure 12e–g. As shown in Figure 12e–g, the superlubric state observed in PTFE–steel ball contacts under graphene-doped silicone oil lubrication results from the formation of a graphene-containing transfer film that lowers shear strength, enhances load-carrying capacity, and maintains stable adhesion during sliding, thereby reducing the COF from 0.26 in dry conditions to as low as 0.008 under high load and speed [88]. At the same time, the electrical mechanisms benefit from the suppression of air breakdown by the nonpolar silicone oil and the channel effect of dispersed graphene nanosheets (Figure 12g), which facilitates electron migration and significantly boosts triboelectric output. Optimal graphene concentrations (around 0.1 wt.%) yield peak short-circuit current and voltage values of 2.42 nA and 0.92 V, while excessive concentrations (0.5 wt.%) cause agglomeration and performance decline. Together, the synergistic solid–liquid coupling of silicone oil and graphene nanosheets enables both macroscale superlubricity and enhanced electrical generation, demonstrating a powerful strategy for high-performance TENG applications [88].

The improvement in the current output and reduction in wear of the TENG based on the PTFE–steel pair under liquid lubrication was explained by Guo et al. [97]. Under dry conditions, the TENG initially shows an increase in current output due to increased frictional triboelectric charges, but the severe wear of the PTFE film occurs, and a transfer film forms on the steel surface, ultimately reducing the PTFE–steel contact and, hence, the output current [97]. In contrast, the TENG performance is improved with hexadecane–OLC lubrication, which minimizes the wear of PTFE, reduces transfer film formation on the steel plate, and maintains effective contact between PTFE and steel, while enabling charge transfer through the liquid film to enhance the surface charge density [97]. The liquid lubricant composed of hexadecane and OLC reduces the air breakdown and lowers the friction, with OLC acting as a micro-bearing [97]. Thus, liquid lubrication suppresses PTFE transfer film formation, improves the contact area, and significantly enhances output efficiency. Figure 12h summarizes the overview of TENG performance in non-lubricant and lubricant conditions.

10. Applications Demonstration of TENGs

TENGs designate a unique approach to obtaining electrical energy by scavenging sustainable environmental energy. Consequently, TENGs have been used to harvest energy from the wind, ocean, and human motions [31,81,83]. Evidence of TENG devices in real-world applications for harvesting sustainable environmental energy is demonstrated through powering electronic devices, smart sensors, emergency message signaling, and performance assessment in sports [31,81,83].

The power-generating ability of the cTENG was demonstrated by harvesting energy from human motion and water waves. In daily life, periodic and non-periodic reciprocating motions are widely present, such as limb movements, engine cylinder operations, water waves, and damping systems [81]. Figure 13a,b show the powering of dozens of LEDs using water wave motion, demonstrating the potential application of the cTENG in water navigation fields for self-powered signal lights, underwater obstruction warning lights, channel lights, and more [81]. Figure 13c–e illustrate the powering of parallel-connected white bulbs simply by shaking the cTENG by hand, thereby harvesting motion energy from the human body [81]. The DLSS–TENG connected to a rectifying diode circuit successfully illuminated 319 LEDs [31]. Similarly, the disk-type DLSS–TENG, when connected to a rectifying diode circuit, was able to charge a commercial capacitor to power electronic devices. With dielectric liquid, the DLSS–TENG charged a 200 μF capacitor up to 1.07 V within 200 s, whereas without dielectric liquid, it charged up to 0.732 V [31]. The charged capacitor was discharged by operating a commercial humidity and temperature sensor with a clock, and then recharged using the DLSS–TENG. This demonstrates the potential application of DLSS–TENG in powering commercial electronic devices from low-input energy sources [31]. Chung et al. [83] demonstrated the practical application of the LLS-TENG, as shown in Figure 13f,g. The prototype and rectification circuit diagram with diodes are shown in Figure 13f, while its high output power illuminated 319 LEDs connected in series and parallel, as shown in Figure 13g. The device's rectified peak current (171 mA) and peak voltage output (220 V) were used to charge different capacitors (100 μF, 200 μF, 300 μF). The LLS-TENG charged 300, 200, and 100 μF capacitors to 1.04, 1.72, and 3.28 V in 200 s, respectively. Moreover, the LLS-TENG charged a commercial lithium-ion battery (3 V, 2 mAh), demonstrating its possible use as a secondary power source for charging commercial storage devices [83].

Zhou et al. [62] demonstrated the enhanced electrical performance of a lubricated rotary sliding FS-TENG compared to a non-lubricated rotary sliding FS-TENG by powering a hygrothermograph and white light bulbs [62]. The rotary sliding FS-TENG was connected to a voltmeter and a capacitor load through a full-wave rectifier. The capacitor voltage was measured using the voltmeter [62]. The charging of 47 μF and 220 μF capacitors by the rotary sliding FS-TENG with and without lubrication at a 1.5 Hz frequency is shown in Figure 13h(i). It can be seen that the voltage of both capacitors reaches 5 V more quickly than in the liquid-lubricated TENG compared to the non-lubricated (air) TENG [62]. For example, the 220 μF capacitor reaches 5 V in 12.9 s under the liquid lubrication, with a corresponding calculated galvanostatic current of 85.13 μA. In contrast, it takes 22.7 seconds for the same capacitor to charge up to 5 V under air conditions, with a corresponding galvanostatic current of 48.4 μA [62]. A hygrothermograph operated by a lubricated and non-lubricated rotary sliding FS-TENGs through a 220 μF capacitor is shown in Figure 13h(ii,iii). Initially, the capacitor voltage declines through the hygrothermograph when the TENGs are in the off state. When TENGs are in an operating mode, the capacitor voltage increases, even while the hygrothermograph is operating. As seen in Figure 13h(iii,iv), the capacitor charges more quickly in the lubricated state of the TENGs compared to the air state while the hygrothermograph is on [62]. Figure 13h(v) shows the lubricated rotary sliding FS-TENG powering four white bulbs connected in sequence, beneath which the text "Triboelectric Nanogenerator" can be clearly seen in the light of the bulbs [62].

A hexadecane–OLC lubricated rotating wheel disc TENG composed of a PTFE–steel pair demonstrated its potential for lighting 50 small LEDs [97]. A ball-bearing-type TENG, composed of three steel balls and three PTFE balls, successfully demonstrated the illumination of 200 LEDs by harvesting rotational mechanical energy. In addition, various capacitors were charged using the ball-bearing TENG operating at 300 rpm. For exam-

ple, a 10 μF capacitor was charged to 0.7 V within 200 s [86]. The rotation-based TENG, consisting of PFA plates and aluminum plates with nonpolar mineral oil lubrication, illuminated 58 serially connected LEDs. This shows that it can generate a continuous electric output and be used as a power source for electronic devices [89]. A rotary freestanding grease-lubricated triboelectric nanogenerator (GL-TENG) demonstrates strong potential for applications in self-sensing and real-time diagnosis of operational states in smart bearings [87]. Building on this concept, Zhao et al. [87] proposed a wireless grease-lubricated triboelectric instantaneous angular speed sensor (GL-TEIASS), which integrates a signal processing circuit specifically designed for bearing fault detection [87]. The developed GL-TEIASS highlights promising prospects for enabling self-sensing capabilities and autonomous operational diagnostics in next-generation smart bearing systems [87]. Wang et al. [92] demonstrated the application of the ORF-TENG by easily powering an "SKLT" design through the arrangement of 50 commercial LEDs.

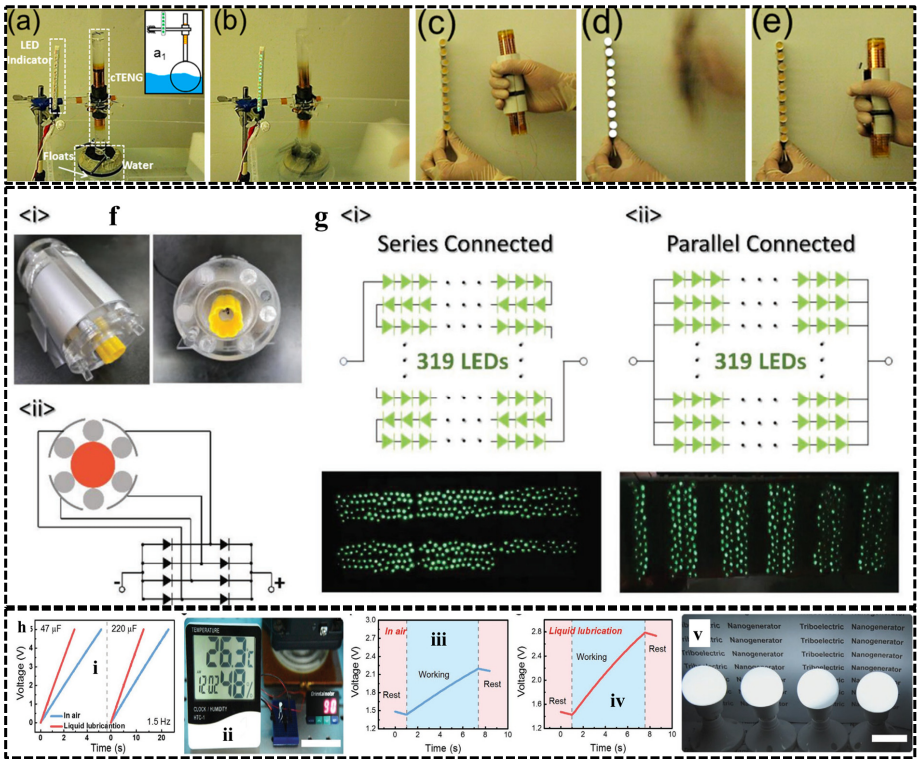


Figure 13. Application demonstration of the cTENG in harvesting reciprocating energy. (**a**) The cTENG was connected to a float to harvest wave energy. The schematic diagram is in (**a1**). (**b**) Green LEDs were lit when an artificial wave passed by. The cTENG was tested with human body motion. White bulbs were driven off-on-off (**c**) before, (**d**) during, and (**e**) after the cTENG was shaken by hand. Reprinted with permission from ref. [81], Copyright (2014), American Chemical Society. The LLS-TENG used as an auxiliary power source. (**f**(**i**)) A Photograph and (**f**(**ii**)) the rectifying circuit configuration of the LLS-TENG, and (**g**) the circuit configuration and a photograph of the illuminated 319 LEDs connected in (**i**) series and (**ii**) parallel. Reprinted with permission from ref. [83], Copyright (2021), Wiley. A demonstration of the rotary sliding FS-TENG as a practical power source. (**h**(**i**)) Charging curves of the capacitor by the rotary FS-TENG in air and with interface liquid lubrication. (**ii**) A photograph of a hygrothermograph driven by the rotary sliding FS-TENG with interface liquid lubrication (scale bar, 5 cm). Charging curves of the capacitor when the hygrothermograph is driven by the rotary FS-TENG in (**iii**) air and with (**iv**) interface liquid lubrication. (**v**) Four white bulbs lighted by the rotary sliding FS-TENG (scale bar, 5 cm). Reprinted with permission from ref. [62], Copyright (2020), Wiley.

The rotational LP-TENG operating at 60 rpm charges various capacitors. For example, the capacitors of 3.3 mF and 1 mF are charged to 5.7 V and 7 V in a short time of 310 s and 104 s, respectively, exhibiting the high charging efficacy [13]. In addition, the rotational LP-TENG lights 1850 LEDs and powers two hygrothermographs when operating at low rotational speeds within the range of 45–60 rpm. Likewise, cell phone charging, motion sensors, light sensors, and power sensors can also be powered by a rotational LP-TENG [13].

A sensor designed using a single-electrode arrayed ERB-TENG demonstrated its practical application in sports activities by assessing the flexibility of juveniles' bodies through the "sit and reach" test. The sensor structure, an electronic circuit with a signal flow chart and complete operation, is illustrated in Figure 14a,b. When the fingers slide across the sensor, it generates the signal, which is subsequently transmitted and processed, finally being displayed on a screen (SDT) and broadcast through a speaker [98]. Thus, the ERB-TENG can be efficiently applied in sports activities to assess performance in the "sit and reach" test.

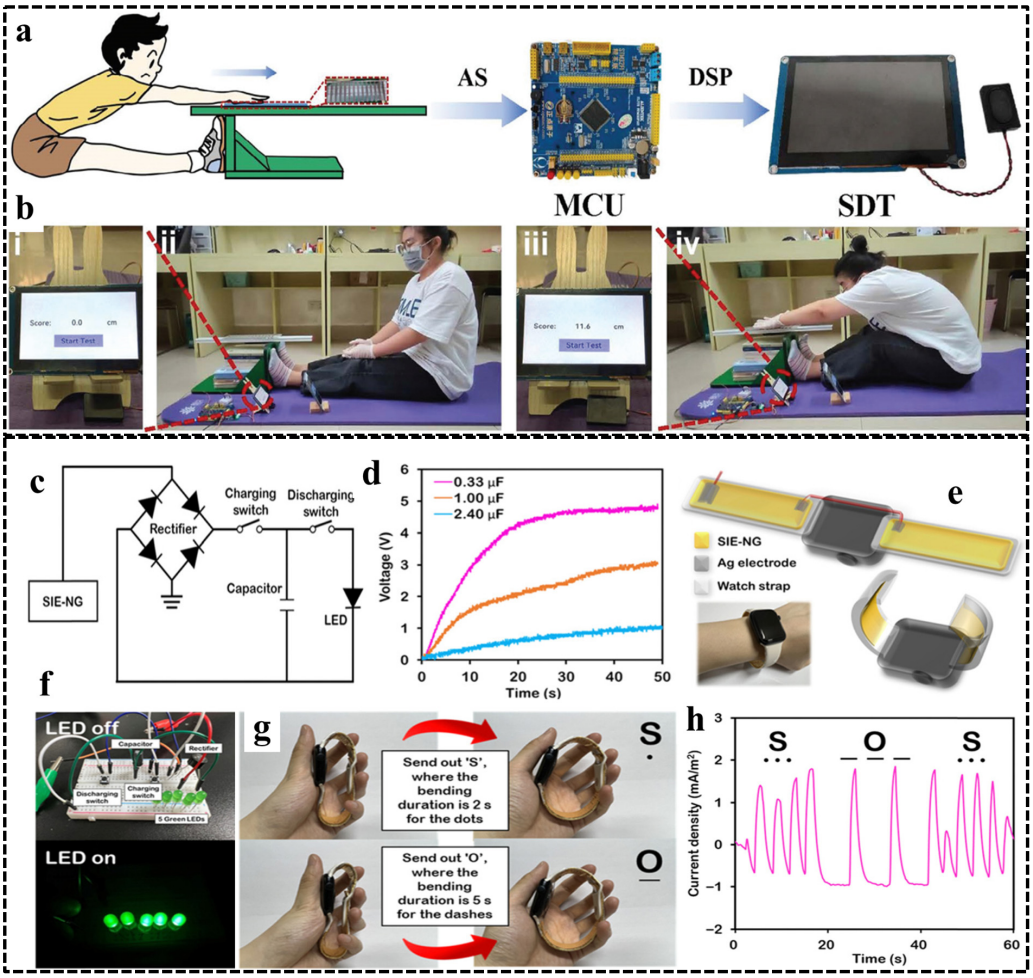


Figure 14. Application demonstrations of the ERB-TENG. (**a**) A signal flowchart of the "sit and reach" intelligence test. (**b**) Demonstrations of the "sit and reach" test system with the ERB-TENG for intelligent sports monitoring. Photographs of the initial state (**i**,**ii**) and status after measurement (**iii**,**iv**). Reproduced from ref. [98] under CC BY 4.0 license. Applications of the SIE-NG: (**c**) a schematic diagram illustrating the electrical circuit for energy storage. (**d**) Capacitor charging using 0.33. 1.00, and 2.40 mF capacitors (strain: 0.2%; frequency: 0.25 Hz). (**e**) A photograph showing the integration of SIE-NG into the watch strap. (**f**) A photograph of the five green LEDs powered by SIE-NG. (**g**,**h**) A photograph showing SIE-NG powering and generating an S.O.S. current signal in Morse code via finger grasping. Reproduced from ref. [3] under CC. BY. 3.0 license.

Zhang et al. [99] successfully demonstrated the potential use of a TAB-TENG to harvest biomechanical energy arising from human stepping motion. Electricity was generated from the reciprocating movement of the heel using a homemade shoe insole, in which the TAB-TENG and the book-shaped handle-driven TENG (BHD-TENG) were fixed [99]. The developed TENG shoe, together with the power transmission circuit, can convert stepping motion energy into electrical energy by lighting a "DHU 70" pattern consisting of 49 red light-emitting diodes (LEDs) connected in series [99]. Finally, an integrated system comprising the BHD-TENG shoe, a microcontroller unit (MCU), and a wireless transmitter was developed for walking state monitoring. An integrated device with a smartphone app visualizes the waking-state monitor. Six indicators update rapidly during walking and stop immediately when walking ceases. These results demonstrate that a smart foot system was successfully constructed and exhibited considerable potential in self-powered intelligent wearable applications [99].

A newly developed Au/PET SIE-NG demonstrated its practical applications by illuminating five LEDs and charging capacitors using ultralow-frequency (<0.2 Hz) mechanical energy (Figure 14c,d,f). The SIG-NG can be seamlessly integrated into a smartwatch strap to generate electricity from the slow movement of the hand (Figure 14e). Remarkably, the SIE-NG device is capable of producing Morse-code signals by harvesting low-frequency mechanical energy generated through watch strap bending during the gradual clenching of fingers (Figure 14g,h). These results underline the potential of SIE-NG as a life-saving device in emergency conditions, offering distinct advantages over conventional TENGs [3].

11. Summary and Perspectives

In this review, we have discussed the four fundamental modes of TENG along with their working mechanism. Among these modes, sliding-mode TENGs exhibit superior electrical output performance over a contact–separation mode. However, although LS- or FS-mode TENGs show this superiority, they still face challenges, such as frictional wear, air breakdown, and low durability. Lubricants play an important role in overcoming these challenges faced by sliding-mode TENGs. The results summarized in this review highlight the advantages of liquid lubricants in TENGs, particularly in the sliding mode, compared to those operating under dry friction. The wear-resistance of the triboelectric polymer materials is significantly enhanced under liquid lubrication, whereas under dry friction, the polymer materials break within a short period of sliding due to severe wear. Liquid lubricants also suppress air breakdown at the contact interface owing to their higher breakdown voltage, thereby increasing the electrostatic fields across the micro-gaps of contact surfaces. Moreover, the electrical performance of TENGs is strongly dependent on the permittivity of the liquid lubricants. The lubricants with low permittivity (e.g., squalane, hexadecane) contribute to enhance electric output of TENGs, while those with high permittivity (e.g., alcohols, water) tend to minimize output performance. Liquid lubricants have shown clear influence on friction, wear, and triboelectric performance. In fact, liquid lubrication enhances the current and voltage output of TENGs while simultaneously minimizing the friction and wear. Nonpolar liquid lubricants, in particular, demonstrate superior triboelectric performance compared with polar liquid lubricants. The stability of liquid-lubricated TENGs is improved remarkably compared to that of non-lubricated TENGs. Nonetheless, sliding-mode TENGs still face challenges in improving electrical performance and achieving an ultralong lifespan.

- Design: Liquid lubrication, while capable of mitigating certain challenges in sliding-mode TENGs, needs a special design, and problems such as leakage or evaporation over time may adversely affect electrical output.

- Not suitable for wearable applications: In addition, although liquid lubricants represent a feasible approach, they complicate device design, making them less convenient for wearable or biomedical applications where simplicity and miniaturization are essential.
- Prolonged Operation: A periodic addition of the liquid lubricant during the prolonged operation is cumbersome in TENG applications, as the lubricant may evaporate due to increased temperature at the contact interface.
- Lubricant Properties: Though lubricants have shown improved performance of TENG in terms of electrical output and durability, their intrinsic properties, such as viscosity, permittivity, conductivity, and dielectric constant, significantly affect their performance.
- Compatibility: The compatibility of liquid lubricants with TENG materials, as well as health and environmental concerns, has received less consideration and needs further exploration. Compared to the liquid lubricant, less attention has been given to the solid or semisolid (grease-like) lubricants.
- Simultaneous measurement of friction and electrical output: Friction is always accompanied by triboelectrification; however, there is still limited research on this phenomenon. Fewer instrumental facilities are available to measure both friction and triboelectricity simultaneously under dry as well as lubrication conditions, and therefore, their correlation has not been fairly established.
- Working mechanism: The lubrication and charge transfer mechanism at the solid–liquid–solid contact interfaces needs further exploration, as current studies do not provide in-depth information.

The primary contribution of the current review lies in identifying key areas for minimizing frictional wear and enhancing the electrical output of TENGs, along with durability. By addressing current issues and outlining effective approaches, this review aims to guide researchers in developing TENG devices that are highly wear-resistant and stable. In addition, an ultrathin, unique, and frictionless SIE-NG device has recently emerged as an alternative to liquid-lubricated or dry friction-based TENGs, attracting significant attention from researchers.

Author Contributions: Conceptualization, P.R.D. and D.-H.C.; writing—original draft preparation, P.R.D.; writing—review and editing, P.R.D. and D.-H.C.; visualization, D.-H.C.; supervision, D.-H.C.; project administration, D.-H.C.; funding acquisition, D.-H.C. All authors have read and agreed to the published version of the manuscript.

Funding: This research was supported by the Basic Science Research Program through the National Research Foundation of Korea (NRF), funded by the Ministry of Education (RS-2023-00239590).

Data Availability Statement: Not applicable. Data was obtained from references.

Conflicts of Interest: The authors declare no conflict of interest.

References

1. Zhang, C.; Mo, J.; Fu, Q.; Liu, Y.; Wang, S.; Nie, S. Wood-cellulose-fiber-based functional materials for triboelectric nanogenerators. *Nano Energy* **2021**, *81*, 105637. [CrossRef]
2. Li, Y.; Xiao, S.; Luo, Y.; Tian, S.; Tang, J.; Zhang, X.; Xiong, J. Advances in electrospun nanofibers for triboelectric nanogenerators. *Nano Energy* **2022**, *104*, 107884. [CrossRef]
3. Moon, J.; Lee, S.-K.; Im, B.; Byun, D.; Cho, D.-H. Strain-induced electrification-based flexible nanogenerator for efficient harvesting from ultralow-frequency vibration energy at 0.5–0.01 Hz. *Energy Environ. Sci.* **2024**, *17*, 8111–8118. [CrossRef]
4. Zhang, W.; Shi, Y.; Li, Y.; Chen, X.; Shen, H. A review: Contact electrification on special interfaces. *Front. Mater.* **2022**, *9*, 909746. [CrossRef]

5. Trinh, V.-L.; Chung, C.-K. Use of triboelectric nanogenerators in advanced hybrid renewable energy systems for high efficiency in sustainable energy production: A review. *Processes* **2024**, *12*, 1964. [CrossRef]
6. Moon, J.; Kang, G.; Im, B.; Kim, J.; Cho, D.-H.; Byun, D. Flapping and powering characteristics of a flexible piezoelectric nanogenerator at Reynolds number range simulating ocean current. *Sci. Rep.* **2022**, *12*, 16465. [CrossRef]
7. Xu, W.; Chen, Q.; Ren, Q.; Li, J.; Chen, Q.; Zhu, C.; Xie, Y.; Li, W. Recent advances in enhancing the output performance of liquid-solid triboelectric nanogenerator (L-S TENG): Mechanisms, materials, and structures. *Nano Energy* **2024**, *131*, 110191. [CrossRef]
8. Meng, Z.; Li, N.; Chen, X. Exploring triboelectric polymers: Strategies for performance optimization and long-term stability. *Small Methods* **2025**, *9*, e01487. [CrossRef]
9. Fan, F.-R.; Tian, Z.-Q.; Wang, Z.L. Flexible triboelectric generator. *Nano Energy* **2012**, *1*, 328–334. [CrossRef]
10. Wu, C.; Wang, A.C.; Ding, W.; Guo, H.; Wang, Z.L. Triboelectric nanogenerator: A foundation of the energy for the new era. *Adv. Energy Mater.* **2019**, *9*, 1802906. [CrossRef]
11. Wang, L.; Yu, J.; Wang, P.; Yang, L.; Yu, X.; Qiu, J.; Tan, K.; Tang, Y.; Guo, Y. Intelligent online sensing of lubricating oil debris via dual-electrode oil-driven triboelectric nanogenerator. *Chem. Eng. J.* **2025**, *503*, 158413. [CrossRef]
12. Tao, X.; Chen, X. Create more and more triboelectric charges on polymer surface. *Fundam. Res.* **2025**, *5*, 1683–1687. [CrossRef] [PubMed]
13. He, W.; Liu, W.; Fu, S.; Wu, H.; Shan, C.; Wang, Z.; Xi, Y.; Wang, X.; Guo, H.; Liu, H.; et al. Ultrahigh performance triboelectric nanogenerator enabled by charge transmission in interfacial lubrication and potential decentralization design. *Research* **2022**, *2022*, 9812865. [CrossRef] [PubMed]
14. Armitage, J.L.; Ghanbarzadeh, A.; Bryant, M.G.; Neville, A. Investigating the influence of friction and material wear on triboelectric charge transfer in metal–polymer contacts. *Tribol. Lett.* **2022**, *70*, 46. [CrossRef]
15. Tian, T.; Zhao, B.; Wang, Y.; Huang, S.; Ju, X.; Fan, Y. First-principles study on interfacial triboelectrification between water and halogen-functionalized polymer surfaces. *Lubricants* **2025**, *13*, 303. [CrossRef]
16. Im, B.; Lee, S.-K.; Kang, G.; Moon, J.; Byun, D.; Cho, D.-H. Electrohydrodynamic jet printed silver-grid electrode for transparent raindrop energy-based triboelectric nanogenerator. *Nano Energy* **2022**, *95*, 107049. [CrossRef]
17. Qin, S.; Yang, P.; Liu, Z.; Hu, J.; Li, N.; Ding, L.; Chen, X. Triboelectric sensor with ultra-wide linear range based on water-containing elastomer and ion-rich interface. *Nat. Commun.* **2024**, *15*, 10640. [CrossRef]
18. Li, N.; Yang, P.; Bai, Z.; Shen, T.; Liu, Z.; Qin, S.; Hu, J.; Yu, C.; Dong, Z.; Chen, X. Bioinspired Electrostatic Capture-and-Release System for Precise Microdroplet Manipulation. *Adv. Mater.* **2025**, *37*, e2418711. [CrossRef]
19. Nie, J.; Ren, Z.; Shao, J.; Deng, C.; Xu, L.; Chen, X.; Li, M.; Wang, Z.L. Self-Powered Microfluidic Transport System Based on Triboelectric Nanogenerator and Electrowetting Technique. *ACS Nano* **2018**, *12*, 1491–1499. [CrossRef]
20. Tremmel, S.; Luo, X.; Rothammer, B.; Seynstahl, A.; Wang, B.; Rosenkranz, A.; Marian, M.; Zhu, L. Evaluation of DLC, MoS2, and Ti3C2T thin films for triboelectric nanogenerators. *Nano Energy* **2022**, *97*, 107185. [CrossRef]
21. Shi, Z.; Zhang, Y.; Gu, J.; Liu, B.; Fu, H.; Liang, H.; Ji, J. Triboelectric nanogenerators: State of the art. *Sensors* **2024**, *24*, 4298. [CrossRef] [PubMed]
22. Zhou, Y.; Zhang, J.-H.; Li, S.; Qiu, H.; Shi, Y.; Pan, L. Triboelectric nanogenerators based on 2D materials: From materials and devices to applications. *Micromachines* **2023**, *14*, 1043. [CrossRef] [PubMed]
23. Deshmukh, P.R.; Cho, D.H. Review of testing configurations for simultaneous measurement of friction and triboelectrification. *Tribol. Lubr.* **2024**, *40*, 118–132.
24. Deshmukh, P.R.; Cho, D.H. Research progress in lubrication and reliability strategies for triboelectric nanogenerators. *Tribol. Lubr.* **2024**, *40*, 281–298.
25. Kwak, S.S.; Yoon, H.; Kim, S. Textile-based triboelectric nanogenerators for self-powered wearable electronics. *Adv. Funct. Mater.* **2019**, *29*, 1804533. [CrossRef]
26. Menge, H.G.; Kim, J.O.; Park, Y.T. Enhanced triboelectric performance of modified pdms nanocomposite multilayered nanogenerators. *Materials* **2020**, *13*, 4156. [CrossRef]
27. Chi, Y.; Xia, K.; Zhu, Z.; Fu, J.; Zhang, H.; Du, C.; Xu, Z. Rice paper-based biodegradable triboelectric nanogenerator. *Microelectron. Eng.* **2019**, *216*, 111059. [CrossRef]
28. Zhang, Z.; Yan, Q.; Liu, Z.; Zhao, X.; Wang, Z.; Sun, J.; Wang, Z.L.; Wang, R.; Li, L. Flexible MXene composed triboelectric nanogenerator via facile vacuum-assistant filtration method for self-powered biomechanical sensing. *Nano Energy* **2021**, *88*, 106257. [CrossRef]
29. Li, Z.; Wang, X.; Fu, T.; Hu, Y.; Li, L.; Zhao, Z.; Wu, L.; Wang, C.; Zhang, S. Research on nano-film composite lubricated triboelectric speed sensor for bearing skidding monitoring. *Nano Energy* **2023**, *113*, 108591. [CrossRef]
30. Wu, J.; Xi, Y.; Shi, Y. Toward wear-resistive, highly durable and high performance triboelectric nanogenerator through interface liquid lubrication. *Nano Energy* **2020**, *72*, 104659. [CrossRef]

31. Chung, J.; Chung, S.-H.; Lin, Z.-H.; Jin, Y.; Hong, J.; Lee, S. Dielectric liquid-based self-operating switch triboelectric nanogenerator for current amplification via regulating air breakdown. *Nano Energy* **2021**, *88*, 106292. [CrossRef]
32. Zhao, Z.; Wang, X.; Hu, Y.; Li, Z.; Li, L.; Ye, G. Investigation on the tribological properties and electrification performance of grease-lubricated triboelectric nanogenerators. *Tribol. Int.* **2024**, *191*, 109163. [CrossRef]
33. Park, S.; Kang, H.; Byun, D.; Cho, D.H. Synthesis and evaluation of superhydrophobic ODA/PDMS dip coating on PET for liquid–solid contact electrification. *Tribol. Lubr.* **2021**, *37*, 71–76.
34. Gong, L.; Zhang, Z.; Yu, W.; Zeng, J.; Cao, J.; Fan, B.; Zhao, J.; Zhang, C. Ultra-durable polysilicon based tribovoltaic nanogenerators for bearing in situ rotational speed sensing. *Small* **2024**, *20*, e2405992. [CrossRef]
35. Thainiramit, P.; Jayasvasti, S.; Yingyong, P.; Nandrakwang, S.; Isarakorn, D. Triboelectric energy-harvesting floor tile. *Materials* **2022**, *15*, 8853. [CrossRef]
36. Bai, Y.; Zhu, W.; Zhang, M.; Hasan, A.M.; Bowen, C.R.; Yang, Y. Triboelectric nanogenerator for harvesting ultra-high-speed wind energy with high-frequency output. *J. Mater. Chem. A* **2025**, *13*, 9101–9110. [CrossRef]
37. Liang, X.; Liu, S.; Yang, H.; Jiang, T. Triboelectric Nanogenerators for Ocean Wave Energy Harvesting: Unit Integration and Network Construction. *Electronics* **2023**, *12*, 225. [CrossRef]
38. Yu, A.; Pu, X.; Wen, R.; Liu, M.; Zhou, T.; Zhang, K.; Zhang, Y.; Zhai, J.; Hu, W.; Wang, Z.L. Core–Shell-Yarn-Based Triboelectric Nanogenerator Textiles as Power Cloths. *ACS Nano* **2017**, *11*, 12764–12771. [CrossRef]
39. Park, S.; Byun, D.; Cho, D.H. Evaluation of h-BN Nanoflakes/Polyimide Composites for a Triboelectric Nanogenerator. *Tribol. Lubr.* **2021**, *37*, 125–128.
40. Wang, Y.-M.; Zhang, X.; Ran, Y.; Liu, C.; Wang, D.; Mao, G.; Jiang, X.; Wang, S.; Yin, X.-B.; Yang, R. Advances in Metal–Organic Framework-Based Triboelectric Nanogenerators. *ACS Mater. Lett.* **2024**, *6*, 3883–3898. [CrossRef]
41. Liang, Y.; Xu, X.; Zhao, L.; Lei, C.; Dai, K.; Zhuo, R.; Fan, B.; Cheng, E.; Hassan, M.A.; Gao, L.; et al. Advances of strategies to increase the surface charge density of triboelectric nanogenerators: A review. *Small* **2023**, *20*, e2308469. [CrossRef]
42. Cao, C.; Li, Z.; Shen, F.; Zhang, Q.; Gong, Y.; Guo, H.; Peng, Y.; Wang, Z.L. Progress in techniques for improving the output performance of triboelectric nanogenerators. *Energy Environ. Sci.* **2023**, *17*, 885–924. [CrossRef]
43. Zhou, Y.; Deng, W.; Xu, J.; Chen, J. Engineering materials at the nanoscale for triboelectric nanogenerators. *Cell Rep. Phys. Sci.* **2020**, *1*, 100142. [CrossRef]
44. Nawaz, A.; Yoon, H.-J. Application of polymer lubricants in triboelectric energy harvesting: A review. *Micromachines* **2025**, *16*, 1195. [CrossRef] [PubMed]
45. Luo, J.; Wang, Z.L. Recent progress of triboelectric nanogenerators: From fundamental theory to practical applications. *EcoMat* **2020**, *2*, e12059. [CrossRef]
46. Wang, S.; Lin, L.; Xie, Y.; Jing, Q.; Niu, S.; Wang, Z.L. Sliding-triboelectric nanogenerators based on in-plane charge-separation mechanism. *Nano Lett.* **2013**, *13*, 2226–2233. [CrossRef]
47. Hu, Y.; Wang, X.; Li, H.; Li, Z.; Sun, N. Tribological properties and electrification performance of patterned surface for sliding-mode triboelectric nanogenerator. *Langmuir* **2019**, *35*, 9396–9401. [CrossRef]
48. Li, Z.; Wang, X.; Hu, Y.; Li, L.; Wang, C. Triboelectric properties of BaTiO3/polyimide nanocomposite film. *Appl. Surf. Sci.* **2022**, *572*, 151391. [CrossRef]
49. Armitage, J.; Ghanbarzadeh, A.; Wang, C.; Neville, A. An investigation into the influence of tribological parameters on the operation of sliding triboelectric nanogenerators. *Tribol. Int.* **2021**, *155*, 106778. [CrossRef]
50. Galembeck, F.; Burgo, T.A.L.; Balestrin, L.B.S.; Gouveia, R.F.; Silva, C.A.; Galembeck, A. Friction, tribochemistry and triboelectricity: Recent progress and perspectives. *RSC Adv.* **2014**, *4*, 64280–64298. [CrossRef]
51. Chung, S.-H.; Chung, J.; Lee, S. Recent advances in lubricant-based triboelectric nanogenerators for enhancing mechanical lifespan and electrical output. *Nanoenergy Adv.* **2022**, *2*, 210–221. [CrossRef]
52. Zhao, J.; Shi, Y. Boosting the durability of triboelectric nanogenerators: A critical review and prospect. *Adv. Funct. Mater.* **2023**, *33*, 2213407. [CrossRef]
53. Li, G.; Yang, S.; Xing, P.; Liu, T.; Gao, H.; Song, Y.; Zhang, H. Experimental investigation of triboelectrification behaviour in the friction process. *Lubricants* **2022**, *10*, 180. [CrossRef]
54. Yang, W.; Wang, J.; Wang, X.; Chen, P. Anisotropic tribology and electrification properties of sliding-mode triboelectric nanogenerator with groove textures. *Friction* **2024**, *12*, 1828–1837. [CrossRef]
55. An, S.; Fu, S.; He, W.; Li, G.; Xing, P.; Du, Y.; Wang, J.; Zhou, S.; Pu, X.; Hu, C. Boosting output performance of sliding mode triboelectric nanogenerator by shielding layer and shrouded-tribo-area optimized ternary electrification layered architecture. *Small* **2023**, *19*, e2303277. [CrossRef] [PubMed]
56. Balasubramaniam, G.; Cho, D.-H. Hexagonal boron nitride nanosheets eco-friendly dispersed in pure water for lubrication in fretting contacts between steel pairs. *Wear* **2023**, 530–531, 205057. [CrossRef]
57. Karluk, A.A.; Ekim, S.D.; Baytekin, B.; Baytekin, H.T. Online lubricant degradation monitoring using contact charging of polymers. *Appl. Surf. Sci.* **2022**, *584*, 152593. [CrossRef]

58. Lee, J.H.; Cho, D.-H.; Park, B.H.; Choi, J.S. Nanotribology of 2D materials and their macroscopic applications. *J. Phys. D: Appl. Phys.* **2020**, *53*, 393001. [CrossRef]
59. Nasser, K.; Guimarey, M.J.G.; Pereira, N.d.M. Recent studies on nanomaterials as additives to lubricants under electrified conditions for tribology: Review. *Lubricants* **2025**, *13*, 2. [CrossRef]
60. Greco, A.; Sheng, S.; Keller, J.; Erdemir, A. Material wear and fatigue in wind turbine Systems. *Wear* **2013**, *302*, 1583–1591. [CrossRef]
61. Balasubramaniam, G.; Cho, D.H. Lubricating effect of water-soluble hexagonal boron nitride nanolubricants on AISI 304 steel sliding pair. *Tribol. Lubr.* **2023**, *39*, 43–48.
62. Zhou, L.; Liu, D.; Zhao, Z.; Li, S.; Liu, Y.; Liu, L.; Gao, Y.; Wang, Z.L.; Wang, J. Simultaneously Enhancing Power Density and Durability of Sliding-Mode Triboelectric Nanogenerator via Interface Liquid Lubrication. *Adv. Energy Mater.* **2020**, *10*, 2002920. [CrossRef]
63. Liu, D.; Zhou, L.; Cui, S.; Gao, Y.; Li, S.; Zhao, Z.; Yi, Z.; Zou, H.; Fan, Y.; Wang, J.; et al. Standardized measurement of dielectric materials' intrinsic triboelectric charge density through the suppression of air breakdown. *Nat. Commun.* **2022**, *13*, 6019. [CrossRef] [PubMed]
64. Kitamura, T.; Kojima, H.; Hayakawa, N.; Kobayashi, K.; Kato, T.; Rokunohe, T. Influence of space charge by primary and secondary streamers on breakdown mechanism under non-uniform electric field in air. In Proceedings of the 2014 IEEE Conference on Electrical Insulation and Dielectric Phenomena (CEIDP), Des Moines, IA, USA, 19–22 October 2014; pp. 122–125.
65. Zhu, J.; Zhu, M.; Shi, Q.; Wen, F.; Liu, L.; Dong, B.; Haroun, A.; Yang, Y.; Vachon, P.; Guo, X.; et al. Progress inTENGtechnology—A journey from energy harvesting to nanoenergy and nanosystem. *EcoMat* **2020**, *2*, e12058. [CrossRef]
66. Tian, Y.; An, Y.; Xu, B. MXene-based materials for advanced nanogenerators. *Nano Energy* **2022**, *101*, 107556. [CrossRef]
67. Potu, S.; Kulandaivel, A.; Gollapelli, B.; Khanapuram, U.K.; Rajaboina, R.K. Oxide based triboelectric nanogenerators: Recent advances and future prospects in energy harvesting. *Mater. Sci. Eng. R Rep.* **2024**, *161*, 100866. [CrossRef]
68. Chen, A.; Zhang, C.; Zhu, G.; Wang, Z.L. Polymer materials for high-performance triboelectric nanogenerators. *Adv. Sci.* **2020**, *7*, 2000186. [CrossRef]
69. Sun, E.; Zhu, Q.; Rehman, H.U.; Wu, T.; Cao, X.; Wang, N. Magnetic material in triboelectric nanogenerators: A review. *Nanomaterials* **2024**, *14*, 826. [CrossRef]
70. Rajaboina, R.K.; Khanapuram, U.K.; Vivekananthan, V.; Khandelwal, G.; Potu, S.; Babu, A.; Madathil, N.; Velpula, M.; Kodali, P. Crystalline porous material-based nanogenerators: Recent progress, applications, challenges, and opportunities. *Small* **2023**, *20*, e2306209. [CrossRef]
71. Thakur, A.; Devi, P. Paper-based flexible devices for energy harvesting, conversion and storage applications: A review. *Nano Energy* **2022**, *94*, 106927. [CrossRef]
72. Ding, Z.; Wang, X.; Huang, C.; Choi, K.; Choi, D. Advances in intelligent sports based on triboelectric nanogenerators. *Nanoenergy Adv.* **2024**, *4*, 258–283. [CrossRef]
73. Bhaduri, A.; Ha, T. Biowaste-derived triboelectric nanogenerators for emerging bioelectronics. *Adv. Sci.* **2024**, *11*, e2405666. [CrossRef] [PubMed]
74. Rodrigues, C.; Nunes, D.; Clemente, D.; Mathias, N.; Correia, J.M.; Rosa-Santos, P.; Taveira-Pinto, F.; Morais, T.; Pereira, A.; Ventura, J. Emerging triboelectric nanogenerators for ocean wave energy harvesting: State of the art and future perspectives. *Energy Environ. Sci.* **2020**, *13*, 2657–2683. [CrossRef]
75. Tian, J.; Chen, X.; Wang, Z.L. Environmental energy harvesting based on triboelectric nanogenerators. *Nanotechnology* **2020**, *31*, 242001. [CrossRef]
76. Jiang, H.; Lv, X.; Wang, K. Application of triboelectric nanogenerator in self-powered motion detection devices: A review. *APL Mater.* **2024**, *12*, 070601. [CrossRef]
77. Dip, T.M.; Arin, R.A.; Anik, H.R.; Uddin, M.; Tushar, S.I.; Sayam, A.; Sharma, S. Triboelectric nanogenerators for marine applications: Recent advances in energy harvesting, monitoring, and self-powered equipment. *Adv. Mater. Technol.* **2023**, *8*, 2300802. [CrossRef]
78. Li, X.; Wei, D.; Wang, Z.L. Direct current triboelectric nanogenerators, a perspective from material selections. *Nanoenergy Adv.* **2023**, *3*, 343–375. [CrossRef]
79. Du, S.; Basset, P.; Guo, H.; Galayko, D.; Karami, A. Power management technologies for triboelectric nanogenerators. *MRS Bull.* **2025**, *50*, 305–314. [CrossRef]
80. Hu, J.; Liu, Z.; Yang, P.; Qin, S.; Li, N.; Ji, W.; Wang, Z.L.; Chen, X. Charge transfer behavior of triboelectric polymers and triboelectric sensors operated under ultrahigh pressure. *Susmat* **2024**, *4*, e250. [CrossRef]
81. Jing, Q.; Zhu, G.; Bai, P.; Xie, Y.; Chen, J.; Han, R.P.S.; Wang, Z.L. Case-Encapsulated Triboelectric Nanogenerator for Harvesting Energy from Reciprocating Sliding Motion. *ACS Nano* **2014**, *8*, 3836–3842. [CrossRef]
82. Zhang, J.; Zheng, Y.; Xu, L.; Wang, D. Oleic-acid enhanced triboelectric nanogenerator with high output performance and wear resistance. *Nano Energy* **2020**, *69*, 104435. [CrossRef]

83. Chung, S.; Chung, J.; Song, M.; Kim, S.; Shin, D.; Lin, Z.; Koo, B.; Kim, D.; Hong, J.; Lee, S. Nonpolar Liquid Lubricant Submerged Triboelectric Nanogenerator for Current Amplification via Direct Electron Flow. *Adv. Energy Mater.* **2021**, *11*, 2100936. [CrossRef]
84. Ariffin, N.A.A.M.; Lee, C.T.; Thirugnanasambandam, A.; Wong, K.J.; Chong, W.W.F. Triboelectric Performance of Ionic Liquid, Synthetic, and Vegetable Oil-Based Polytetrafluoroethylene (PTFE) Greases. *Lubricants* **2024**, *12*, 272. [CrossRef]
85. Abozeid, A.A.; Youssef, M.M.; Megahed, T.F.; El-Helaly, M.; Pape, F.; Nassef, M.G.A. Tribo-Electric Performance of Nano-Enhanced Palm Oil-Based Glycerol Grease for Electric Vehicle Bearings. *Lubricants* **2025**, *13*, 354. [CrossRef]
86. Song, M.; Chung, J.; Chung, S.-H.; Cha, K.; Heo, D.; Kim, S.; Hwang, P.T.; Kim, D.; Koo, B.; Hong, J.; et al. Semisolid-lubricant-based ball-bearing triboelectric nanogenerator for current amplification, enhanced mechanical lifespan, and thermal stabilization. *Nano Energy* **2022**, *93*, 106816. [CrossRef]
87. Zhao, Z.; Wang, X.; Hu, Y.; Li, Z.; Li, L.; Wu, L. Grease-lubricated triboelectric instantaneous angular speed sensor integrated with signal processing circuit for bearing fault diagnosis. *Nano Energy* **2023**, *117*, 108871. [CrossRef]
88. Chen, J.; Zhao, Y.; Wang, R.; Wang, P. Super-Low Friction Electrification Achieved on Polytetrafluoroethylene Films-Based Triboelectric Nanogenerators Lubricated by Graphene-Doped Silicone Oil. *Micromachines* **2023**, *14*, 1776. [CrossRef] [PubMed]
89. Lee, J.; Chung, S.-H.; Kim, B.; Son, J.-H.; Lin, Z.-H.; Lee, S.; Kim, S. Wear and triboelectric performance of polymers with non-polar lubricants. *Tribol. Int.* **2023**, *178*, 108088. [CrossRef]
90. Wang, K.; Li, J.; Li, J.; Wu, C.; Yi, S.; Liu, Y.; Luo, J. Hexadecane-containing sandwich structure based triboelectric nanogenerator with remarkable performance enhancement. *Nano Energy* **2021**, *87*, 106198. [CrossRef]
91. Shi, W.; Wang, X.; Diao, W.; Liu, G.; Cao, Y. Effect of pump voltage on triboelectric properties and air breakdown of sliding-mode triboelectric nanogenerator. *Nano Energy* **2025**, *137*, 110758. [CrossRef]
92. Wang, K.; Wu, C.; Zhang, H.; Li, J.; Li, J. Cylindrical bearing inspired oil enhanced rolling friction based nanogenerator. *Nano Energy* **2022**, *99*, 107372. [CrossRef]
93. Liu, X.; Zhang, J.; Zhang, L.; Feng, Y.; Feng, M.; Luo, N.; Wang, D. Influence of interface liquid lubrication on triboelectrification of point contact friction pair. *Tribol. Int.* **2022**, *165*, 107323. [CrossRef]
94. Shao, J.; Yu, G.; He, Y.; Li, J.; Hou, M.; Wang, X.; Zhang, P.; Wang, X. An Investigation of the Output Performances of a Triboelectric Nanogenerator Lubricated with TiO_2-Doped Oleic Acid. *Lubricants* **2024**, *12*, 269. [CrossRef]
95. Wang, K.; Wang, X.; Sun, Y.; Wu, Z.; Zhang, H.; Xiao, K.; Du, J.; Li, J.; Luo, J. Macroscopic liquid superlubric triboelectric nanogenerator: An in-depth understanding of solid-liquid interfacial charge behavior. *Nano Energy* **2024**, *129*, 110038. [CrossRef]
96. Yang, D.; Zhang, L.; Luo, N.; Liu, Y.; Sun, W.; Peng, J.; Feng, M.; Feng, Y.; Wang, H.; Wang, D. Tribological-behaviour-controlled direct-current triboelectric nanogenerator based on the tribovoltaic effect under high contact pressure. *Nano Energy* **2022**, *99*, 107370. [CrossRef]
97. Guo, Y.; Zhang, L.; Du, C.; Feng, Y.; Yang, D.; Zhang, Z.; Feng, M.; Wan, Y.; Wang, D. Onion-like carbon as nano-additive for tribological nanogenerators with enhanced output performance and stability. *Nano Energy* **2022**, *104*, 107900. [CrossRef]
98. Liu, M.; Zhang, X.; Xin, Y.; Guo, D.; Hu, G.; Ma, Y.; Yu, B.; Huang, T.; Ji, C.; Zhu, M.; et al. Earthworm-Inspired Ultra-Durable Sliding Triboelectric Nanogenerator with Bionic Self-Replenishing Lubricating Property for Wind Energy Harvesting and Self-Powered Intelligent Sports Monitoring. *Adv. Sci.* **2024**, *11*, e2401636. [CrossRef]
99. Zhang, X.; Liu, M.; Zhang, Z.; Min, H.; Wang, C.; Hu, G.; Yang, T.; Luo, S.; Yu, B.; Huang, T.; et al. Highly Durable Bidirectional Rotary Triboelectric Nanogenerator with a Self-Lubricating Texture and Self-Adapting Contact Synergy for Wearable Applications. *Small* **2023**, *19*, e2300890. [CrossRef]
100. Cho, D.-H.; Park, S.; Im, B.; Kim, Y.; Kim, S.-W.; Lee, S.-K.; Byun, D. Eco-friendly mass production of MoS_2 flakes in pure water for performance enhancement of triboelectric nanogenerator. *Appl. Surf. Sci.* **2023**, *625*, 157235. [CrossRef]
101. Cho, D.H.; Park, S. Work Function of Water-Exfoliated Hexagonal Boron Nitride Flakes. *Tribol. Lubr.* **2025**, *41*, 143–147.

Disclaimer/Publisher's Note: The statements, opinions and data contained in all publications are solely those of the individual author(s) and contributor(s) and not of MDPI and/or the editor(s). MDPI and/or the editor(s) disclaim responsibility for any injury to people or property resulting from any ideas, methods, instructions or products referred to in the content.